

JGR Atmospheres

RESEARCH ARTICLE

10.1029/2020JD033745

Key Points:

- X-ray bursts were detected simultaneously with a lightning imaging obtained with a very high frequency (VHF) broadband interferometer
- A strong temporal correspondence has been observed between the high-energy radiation and the most intense VHF pulses
- Measurements suggest an extensive spatial origin of Terrestrial Gamma-ray Flashes (TGFs) due to a multiplicity of high-energy sources

Supporting Information:

Supporting Information may be found in the online version of this article.

Correspondence to:

M. Urbani,
michele.urbani@upc.edu

Citation:

Urbani, M., Montanyà, J., Van der Velde, O. A., López, J. A., Arcanjo, M., Fontanes, P., et al. (2021). High-energy radiation from natural lightning observed in coincidence with a VHF broadband interferometer. *Journal of Geophysical Research: Atmospheres*, 126, e2020JD033745. <https://doi.org/10.1029/2020JD033745>

Received 21 AUG 2020
Accepted 15 MAR 2021

High-Energy Radiation From Natural Lightning Observed in Coincidence With a VHF Broadband Interferometer

M. Urbani¹ , J. Montanyà¹ , O. A. van der Velde¹ , J. A. López¹ , M. Arcanjo¹ , P. Fontanes¹ , D. Romero¹ , and J. A. Roncancio¹ 

¹Electrical Engineering Department, Universitat Politècnica de Catalunya, Barcelona, Spain

Abstract This work presents the first simultaneous X-ray measurements from natural lightning in coincidence with a very high frequency (VHF) broadband interferometer. During an observational campaign in north-central Colombia, five intense X-ray bursts were detected from negative stepped leaders and two X-ray emissions from a dart leader. Thanks to the high angular and time resolution of the interferometer, it was possible to locate the origin of high-energy radiation during the lightning leader propagation. We study the correlation with VHF pulses and the two-dimensional speed of the leader channels. A strong temporal correspondence has been observed between the high-energy emissions and the most intense VHF pulses, which suggests the runaway electrons as a shared mechanism. The observations show that an X-ray burst can have multiple high-energy sources belonging to different leader branches, that can be several hundreds of meters apart. Therefore, from a spatial point of view, not a unique origin has to be searched, but an extensive origin of the X-ray burst should be considered. We hypothesize similar conclusions in particular for downward TGFs and maybe for TGFs in general.

Plain Language Summary It is well known that lightning can produce high-energy emissions. In particular, a phenomenon has been observed from space called “Terrestrial Gamma-ray Flash (TGF),” which consists of an intense burst of gamma radiation that can be produced during thunderstorms. This phenomenon has met with considerable interest in the scientific community and its mechanism is still not fully understood. Beyond space observations, in order to investigate TGFs, ground-based measurements can provide complementary information to better understand under which conditions high-energy emissions are produced. In this research context, this work presents some accurate ground-based observations of the location of high-energy emissions during natural cloud-to-ground lightning.

1. Introduction

The first scientific evidence that lightning can emit high-energy radiation was the discovery of a phenomenon observed from space called “Terrestrial Gamma-ray Flash” (TGF). This phenomenon consists on an intense burst of gamma radiation and it was detected for the first time by the Burst and Transient Source Experiment (BATSE) onboard the Compton Gamma-Ray Observatory (CGRO) satellite (Fishman et al., 1994).

The origin of TGFs remained uncertain for many years. It was hypothesized that TGFs were associated with discharges in the upper atmosphere such as sprites (Nemiroff et al., 1997), but ground-based measurements conducted during thunderstorms by Moore et al. (2001) revealed a clear correlation between high-energy emissions and lightning leader propagation. In particular, in 2003, a ground-level gamma-ray flash was observed in a rocket-triggered lightning (Dwyer et al., 2004) with a similar duration and energy spectrum of a TGF detected from space. These observations introduced lightning as a candidate to the origin of the TGF and further models and observations confirm that TGFs are produced inside or just above thunderclouds (Dwyer & Uman, 2014). It is well established that the high-energy radiation is produced by accelerated electrons via bremsstrahlung, but the exact process that generates the high number of runaway electrons needed to justify the observed TGF brightness is still debated (Celestin & Pasko, 2011; Dwyer, 2008, 2020). Two main theories were proposed to explain the TGF origin, the electron acceleration mechanism and the multiplication factor. The first theory, supported by ground-based observations, claims that the intense electric field ahead of the streamer tips might accelerate thermal electrons to runaway during the stepping lightning

leaders (e.g., Celestin & Pasko, 2011; Chanrion & Neubert, 2010; Cummer et al., 2005; Dwyer, 2004; Dwyer, 2008; Carlson et al., 2009; Moss et al., 2006; Williams et al., 2006).

The second theory identifies in cosmic rays the source of the high-energy electrons, named “seeds,” able to trigger the relativistic runaway electron avalanche (RREA) process in thunderstorm ambient electric field (Gurevich et al., 1992). However, the RREA was estimated to not be enough to explain TGFs so an additional mechanism was required to provide enough amplification. In 2003, Dwyer (2003) introduced the “relativistic feedback” a new mechanism involving backward propagating runaway positrons to self-sustain the production of runaway electrons (e.g., Dwyer & Smith, 2005; Dwyer, Smith, & Cummer, 2012; Skeltved et al., 2014). In order to establish which mechanism is dominant and reach a deeper understanding of these high-energy phenomena, more observations are needed.

Currently, two satellites for astrophysics: AGILE and Fermi are able to detect and catalog TGFs (Maiorana et al., 2020; Marisaldi et al., 2014; Von Kienlin et al., 2014) and a specific instrument like the *ASIM-MXGS* detector (Neubert et al., 2020) on the International Space Station are studying TGFs from space. In the atmosphere, the high-energy radiation undergoes a strong absorption, exponentially proportional to the density of the air, which makes it more difficult to detect TGFs on the ground. Nonetheless, several ground measurements were conducted and observed that even in cloud-to-ground (CG) lightning high-energy radiation could be produced.

The works of Moore et al. (2001) and Dwyer et al. (2005) highlight two lightning processes in which the X-ray bursts could be produced: Downward stepped leader and dart leader. The correlation with leader-step electric field derivative and the X-ray emission observed by Dwyer et al. (2005) was confirmed by the measurements of Howard et al. (2008) and Hill (2012). Hill located the X-ray sources in 3D via time-of-arrival techniques for dart-stepped leader steps in both natural and triggered lightning. Three-dimensional Radio Frequency (RF) and X-ray measurements were conducted in natural lightning during the attachment process (Howard et al., 2010) and leader bursts were identified as the largest X-ray producers.

In a triggered lightning experiment (Saleh et al., 2009), measurements showed results compatible with isotropic radiation. Instead, further observations suggested that the X-ray emissions may be beamed to some degree in the direction of the leader propagation and strong VHF emissions were observed (Montanyà et al., 2012). The spatial, energy and angular distribution of the high-energy radiation was debated in (Schaal et al., 2013).

A statistical study of X-ray emissions was published by Mallick et al. (2012) with emphasis on subsequent strokes, they observed that not all leaders of the same flash produced detectable X-rays. Due to the lower air density and consequently lower X-ray absorption, observations of high-energy radiation from thunderstorms were conducted at high-altitude towers (e.g., Hettiarachchi et al., 2018; Montanyà et al., 2014) and on aircraft (e.g., Kochkin et al., 2017; Skeie et al., 2020; Smith et al., 2011). Recently, Saba et al. (2019) measured X-ray emissions in coincidence with a dart leader using high-speed video and pointing out the role of the leader orientation in the X-ray detection.

Currently, it is not clear if the X-ray emissions detected at ground level and the TGFs observed in space are essentially the same phenomenon or how these phenomena are related (e.g., Dwyer, Smith, & Cummer, 2012; Gurevich et al., 2007).

It is relevant to note that several authors named as TGFs (or downward TGFs) their high-energy observations. Two TGFs cases were reported from rocket-triggered lightning (Dwyer et al., 2004; Hare et al., 2016), and other two cases in association with negative CG lightning (Dwyer, Schaal, et al., 2012; Tran et al., 2015) in Florida (USA). Gamma ray glows and downward TGFs were also observed from ground during Japanese winter thunderstorms (e.g., Smith et al., 2018; Wada et al., 2019).

Recently, several ground-based observations of downward TGF were reported from the Telescope Array in Utah (USA) (Abbasi et al., 2017, 2018, 2019). The Telescope Array is a cosmic ray observatory which consists of a large array of more than 500 plastic scintillators of 3 m² deployed in a square grid with 1.2 km spacing. A total of 15 TGFs were observed in the first 1–2 ms of downward negative breakdown prior to cloud-to-ground lightning strikes (Abbasi et al., 2019). The array detectors revealed that the high-energy radiation is forward-beamed and it produces a footprint of 3–5 kilometers in diameter. The observed energy

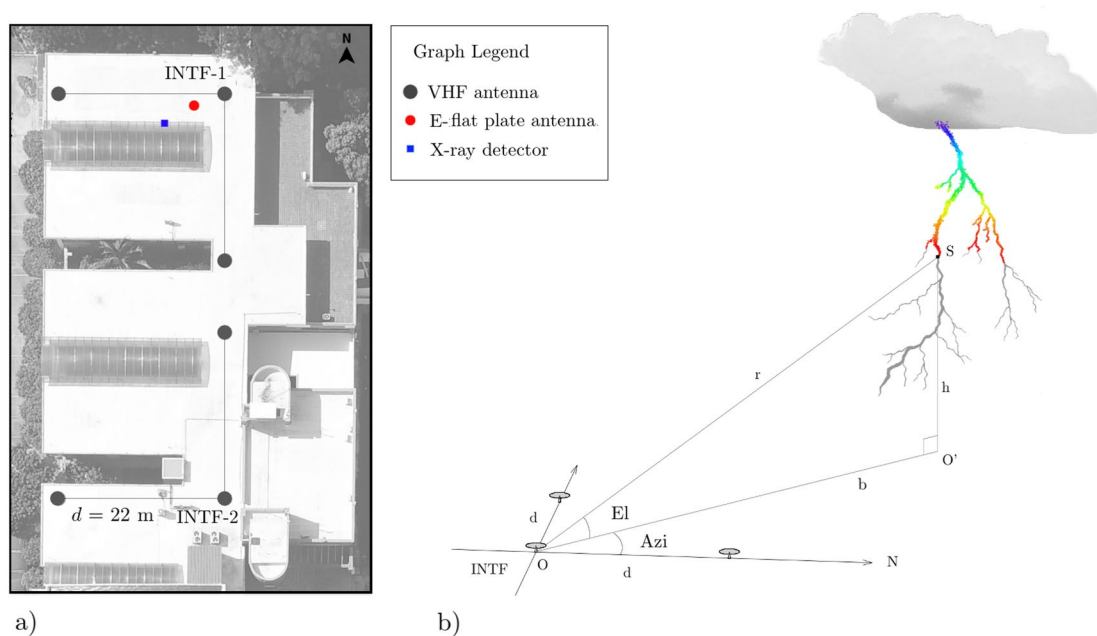


Figure 1. (a) Instrumentation deployment on the UIS roof in Barrancabermeja (Colombia). Two lightning interferometers (INTF), a flat plate antenna for E-field measurements and an X-ray detector. (b) Conceptual scheme and basic geometry of the lightning interferometer. A single interferometer provides a 2D imaging of the lightning in angular coordinates: Elevation and azimuth.

deposit of the gamma ray shower found is consistent with a fluence of 10^{12} – 10^{14} photons. Simulations on the beaming geometries, the fluence, and the time dispersion were discussed by (Berge & Celestin, 2019). These downward TGF observations show that it is particularly interesting and promising to study high-energy emissions also from ground-based instruments. Despite the strong absorption of the high-energy radiation, ground-based observations can reach a better accuracy in time and space and provide crucial information to investigate the origin and conditions under which these emissions occur.

A privileged instrument for this research is a VHF Broadband Lightning Interferometer, a system of antennas that allows to map lightning through the VHF emission. An extensive description of this instrument and its performance it has been provided by Stock et al. (2014). Due to the high resolution of this instrument, it is possible to locate the origin of the high-energy emissions and hopefully provide a better understanding of the radiation mechanism.

2. Instrumentation and Methodology

The measurements reported were made during an observational campaign at the Universidad Industrial de Santander (UIS) campus of Barrancabermeja (Colombia) in autumn 2019. On this site, two lightning interferometer (INTF-1 and INTF-2) were installed and synchronized with a flat-plate antenna, a high-energy detector and a GPS receiver. Figure 1 shows the deployment of the instrumentation on the roof of the university main building.

2.1. VHF Broadband Interferometry System

Lightning discharges emit electromagnetic radiation over a broad range of the electromagnetic spectrum from extremely low frequency (ELF) to gamma-ray energy. In particular, in the VHF band (30–300 MHz) the nature of this emission is characterized by pulses of variable duration from some nanoseconds to a few microseconds. Due to their short duration, it is possible to consider, in first approximation, these pulses as stationary point sources. This assumption allows to locate the VHF sources evaluating the different time-of-arrival (TOA) or the phase difference of the electromagnetic waves detected by a system of antennas.

A VHF broadband lightning interferometer (INTF) is an instrument that allows to map these VHF sources with an interferometric technique called generalized cross-correlation.

Computing the geometric delay δt_{ij} between pairs of antennas with baseline d , it is possible to determine the direction of the point source through two angles: Azimuth and elevation.

$$\begin{aligned} Azi &= \arctan\left(\frac{\delta t_{12}}{\delta t_{13}}\right) \\ El &= \arccos\left(\frac{c}{d}\sqrt{\delta t_{12}^2 + \delta t_{13}^2}\right) \end{aligned} \quad (1)$$

An illustration with the basic geometry of the lightning interferometer is depicted in Figure 1b.

An excellent description of this kind of instrument and the processing technique was presented by the New Mexico Tech researchers (Stock et al., 2014). Our system and processing technique is clearly inspired by their work and we refer further details on the overall operation of the interferometer to their report (Stock et al., 2014).

Two almost identical interferometers were built and developed in order to lead this investigation. Each interferometer consists of three antennas (aluminum disks of radius 20 cm) deployed along two orthogonal baselines ($d = 22$ m). The antenna's output signal is connected to a bandpass-filter (20–80 MHz) and then preamplified. All the antennas are connected using three identical high-quality coaxial cables ($l = 30$ m) to the acquisition system. The hardware of the acquisition system is primarily made by a digitizer and a workstation with sufficient CPU and memory requirements. The digitizer board used is the *GaGe Razor Express 1604*: 4 channel with 16-bit of resolution and 200MS/s of sampling rate and 8 GB of memory. In order to maximize the chance to record interesting events, we developed the acquisition system software to get a *continuous recording* in streaming mode, filling a circular buffer in the RAM memory. We set our acquisition time duration at 2.5 s with 0.5 s of pre-trigger and less than 20 s of dead time after the triggered event.

Both interferometers were online and could be turned on remotely when a storm was approaching. Once activated, the acquisition system can be triggered by an E-field flat plate antenna installed nearby. The flat-plate antenna measures the environmental electric field along the vertical axis. In order to study the high-energy emissions, we were interested in close lightning CG strokes in a 10 km area. For this reason, the gain of the antenna was set properly to avoid saturation and the trigger threshold was adjusted to avoid to collect too remote events. The nominal calibration of the antenna is 16 kV/m on output volt with a time-constant of 1 s. The E-field signal was acquired in the fourth channel of the GaGe digitizer and by a Picoscope PS4424 to synchronize the high-energy detector output with the VHF signals (further details in 2.2).

In the data processing, we applied a window-based cross-correlation method in frequency domain, with up-sampling and parabolic interpolation of the cross-correlation peak. The window length was set to 128 samples (~ 640 ns) with a sliding step of a single sample. To mitigate the effect of the strong window overlapping, a clustering algorithm was applied. We selected all the compatible values within 1 nanosecond and then averaged them together. Several thresholds were applied to improve the accuracy and the noise reduction: An amplitude threshold of the cross-correlation peak of 0.8, a threshold on the closure parameter of 0.6 ns and a minimum size of the cluster of 8 windows. Further details on the data processing and especially a discussion on the imaging efficiency are available in Supporting Information.

2.2. High-Energy Detector

The high-energy detector was installed nearby the INTF-1 (Figure 1a) and it is composed of a NaI(Tl) cylindrical scintillator 76×76 mm (Scionix: Type 76B76/3M-E2-X2) with a photomultiplier tube (PMT). The detector contained a voltage divider and a preamplifier in a magnetic shielded housing and the scintillator is enveloped in an aluminum body (thickness 0.5 mm). The nominal decay constant is 0.23 ms and the rise time $0.5 \mu\text{s}$, in good agreement with measured values. The detector was calibrated in energy at the nuclear physics laboratory in the Physics department at the Polytechnic University of Catalonia (UPC) with a ^{137}Cs and a ^{60}Co radioactive sources. The linear calibration in the range (0–1332 keV) provided a scale factor of

$m = 4.63 \pm 0.02$ keV/mV. This calibration was used, as well, at higher energy assuming a linear response. The output signal was acquired by a Picoscope PS4424 with 12-bit resolution and a sampling rate of 10 MS/s and triggered by the E-field flat plate antenna. Therefore, the acquisition system has two different digitizers with two different sampling rates: The GaGe Board with 4 channels at 200MS/s (3 VHF antennas, E-field flat plate antenna) and the Picoscope 4 channels at 10 MS/s (E-field flat plate antenna, high-energy detector, GPS signal). The E-field signal provides the trigger of both acquisition system and allows an accurate synchronization ($\sim 0.1 \mu\text{s}$) during the post-processing phase. Other systematic instrumental uncertainties were evaluated, all of them are dominated by the rise time of the detector and the synchronization accuracy.

From the signal processing, two relevant quantities are estimated: The X-ray energy and the time-of-arrival t_0 . The energy is evaluated by computing the ΔV of the signal at the pulse rise and then using the calibration factor. This method underestimates the energy when the time interval between two successive pulses is less than the decay time (Bolic et al., 2009). In contrast, an energy overestimation occurs when it is not possible to resolve multiple photons. The resolution to exclude the photon pile-up is dominated by the rise time $\delta t_r \sim 0.5 \mu\text{s}$. Both cases are very common in the physical phenomenon investigated; therefore, with our instrumentation, a very accurate measurement of the energy is out of our scope. On the other hand, an accurate evaluation of the t_0 is crucial for the discussion of the results. For this reason, we applied an algorithm to compute the t_0 using a linear interpolation of the rise time (further details are available in the Supporting Information), this simple procedure ensures a good accuracy and objectivity of the results. Another relevant observation concerns the environmental background. The probability of observing k background pulses in a given time interval Δt can be estimated using the Poisson distribution (e.g., Tran et al., 2019):

$$P(k, \Delta t) = \frac{(\lambda \Delta t)^k e^{-\lambda \Delta t}}{k!} \quad (2)$$

where λ is the average rate of background events and Δt is expressed in milliseconds. We evaluated λ in the field during the campaign and we estimated a mean value of $\lambda = 0.20 \pm 0.05$ events/ms, almost the double of the Mallick et al. (2012) measurements. For example, the probability to have more than 2 background events in the last millisecond before a lightning return stroke is $P(k > 2, 1) \approx 0.001$. Therefore, when a X-ray burst is observed, there is no doubt that those emissions can be related to lightning activity. On the other hand, a single pulse emission has to be evaluated more carefully considering the probability of a false coincidence with lightning activity. (e.g., the chance to have a background pulse in 1 ms before the return stroke is $P(1, 1) \approx 0.18$ and in 0.1 ms is $P(1, 0.1) \approx 0.02$).

2.3. LINET

Complementary data and information to our measurements were provided by the Colombian Total Lightning Detection Network, operated by *Keraunos* company since 2011. This network is composed of 19 low frequency (VLF/LF) sensors of LINET type (Betz et al., 2009) deployed with baselines of approximately 100 km. Further details on this network can be found in Aranguren et al. (2017).

3. Observations and Analysis

During the campaign period, nine thunderstorms were observed and in four of them high-energy radiation was detected. More than 200 lightning events (about 65% CG and 35% IC) triggered the acquisition system and in particular, seven X-ray bursts were detected, of which five intense bursts (with at least ten X-ray pulses) and other 15 lightning events with at least a single X-ray pulse in the last 0.1 ms before the returned stroke were recorded. In order to present the observations, we decided to give an overview of the overall data to contextualize the measurements and then present in detail the most interesting cases.

3.1. Overall Data Analysis

In this paper, an “X-ray burst” is defined as a sequence of three or more X-ray pulses related with the same lightning event. Each X-ray pulse is not necessarily a single photon and the choice of three as the minimum size of an X-ray burst is discussed in Section 2.2. In the literature, it is equally common to define

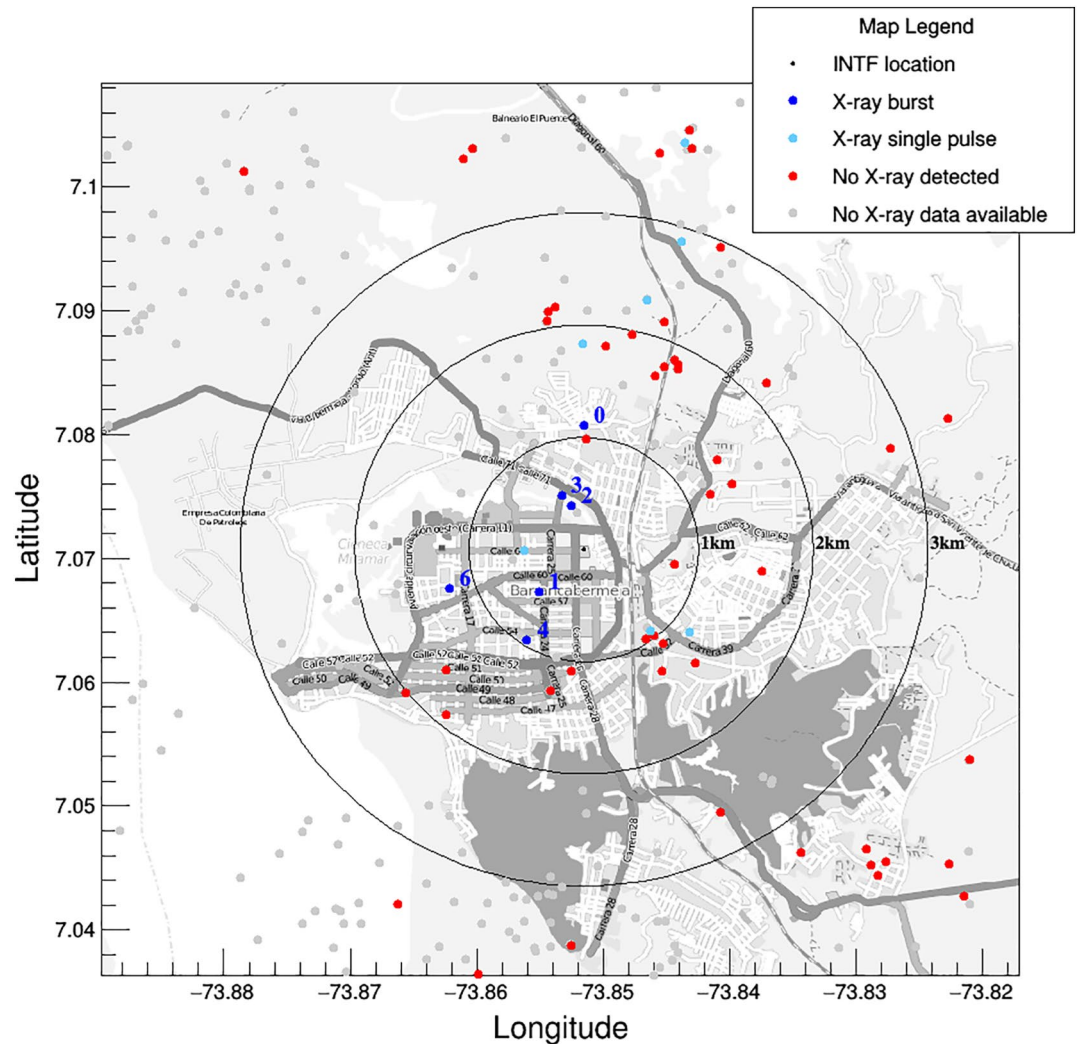


Figure 2. The map shows the LINET lightning location recorded during the observational campaign at the Universidad Industrial de Santander (UIS) campus of Barrancabermeja (Colombia) in autumn 2019. The map is centered in the INTF location. Lightning events observed by the INTF in coincidence with an X-ray burst were colored in blue, lightning events observed by the INTF without X-ray detection were colored in red, lightning events not recorded were colored in gray.

an X-ray burst as the sub-microsecond emissions of multiple energetic photons (e.g., Dwyer et al., 2005). We call “X-ray pulses” the detection of these emissions, as they appear in our measurements (e.g., Mallick et al., 2012).

The observed events can be divided into four categories: (1) Events where an X-ray burst was observed; (2) Events where one or two X-ray pulses were observed (we call these events “single X-ray pulses” as discussed in Section 2.2.); (3) Events in which no X-ray emissions were observed; (4) Events that did not trigger our data acquisition system, but they were recorded by LINET.

In Figure 2 we combined the high-energy detections with the lightning locations provided by LINET. The map is centered in the INTF-1 system of reference and allows to evaluate in particular the radial distance between our detection system and the lightning strokes. It can be observed that all the X-ray bursts detected are within an area delimited by a radius of about 1.2 km, and the majority of the events observed in this area have produced detectable high-energy radiation.

Table 1
X-Ray Bursts Overall Data

X-ray burst ID	Timestamp (UTC)	Distance	Current	Nr. of X-ray pulses
0 ^a	2019-11-11 06:21:52.193	1.10 km	−55.5 kA	3
1	2019-11-11 06:38:16.378	0.55 km	−36.6 kA	23
2	2019-11-11 06:39:06.518	0.40 km	−6.8 kA	22
3	2019-11-11 06:53:03.843	0.52 km	−23.3 kA	4
4	2019-11-11 06:59:04.632	0.95 km	−18.4 kA	10
5 ^b	2019-11-11 07:04:32.823	- km	- kA	11
6	2019-12-31 08:18:23.579	1.22 km	−43.8 kA	11

Distance, current, and timestamp are provided by Keraunos LINET lightning location network.

^aINTF data not available. ^bLINET data not available. GPS timestamp.

Table 1 summarizes the overall X-ray bursts data combining the high-energy measurements with the LINET data. Seven X-ray bursts were observed, corresponding to a total of 84 X-ray pulses. Unfortunately, for some events, we only have some partial data, due to the failure of the trigger in the acquisition system or to the detection efficiency of the lightning network.

Figure 3 shows the energy distribution and the time distribution of the X-ray pulses belonging to the X-ray bursts. The energy distribution has the most frequent count in the range 100–150 keV and the median value is approximately 280 keV. It is possible to observe that the vast majority of the X-ray pulses has an energy below 1 MeV. Higher values of energy have been observed from 2 MeV up to 8 MeV, but these results have to be discussed. Although energies of some MeV can actually be achieved and therefore observed, it is important to underline that our instrument has a rise time of 0.5 μ s and therefore, as explained in Section 2.2, we cannot exclude that some of these values may be due to a pile-up phenomenon caused by the detection of multiple photons (Dwyer, 2004). This energy spectrum is consistent with earlier lightning observations (e.g., Arabshahi et al., 2015; Dwyer et al., 2004) and it is softer than a typical TGF spectra detected from space (e.g., Marisaldi et al., 2014; Østgaard et al., 2012). The time distribution shows a clear increase in X-ray detection approaching the return stroke (RS), as previously observed by Mallick et al. (2012). Unfortunately, with our instrumentation, we are not able to say if this effect is mainly due to the leaders' approach to the ground or due to the decreasing distance between leaders and the high-energy detector. We cannot separate efficiently the two contributions. The maximum duration of the observed X-ray bursts was about 900 μ s and the mean duration \sim 600 μ s. Taking into account the time distribution of all X-ray pulses belonging to the X-ray bursts observed, the median value was 150 μ s before the return stroke.

hi et al., 2015; Dwyer et al., 2004) and it is softer than a typical TGF spectra detected from space (e.g., Marisaldi et al., 2014; Østgaard et al., 2012). The time distribution shows a clear increase in X-ray detection approaching the return stroke (RS), as previously observed by Mallick et al. (2012). Unfortunately, with our instrumentation, we are not able to say if this effect is mainly due to the leaders' approach to the ground or due to the decreasing distance between leaders and the high-energy detector. We cannot separate efficiently the two contributions. The maximum duration of the observed X-ray bursts was about 900 μ s and the mean duration \sim 600 μ s. Taking into account the time distribution of all X-ray pulses belonging to the X-ray bursts observed, the median value was 150 μ s before the return stroke.

3.2. Negative Downward Leaders: 2019-11-11 06:39:06

On November 11, 2019, a tropical thunderstorm passed through Barrancabermeja during the night and several lightning events were recorded. Six X-ray bursts and five X-ray single pulses were detected from

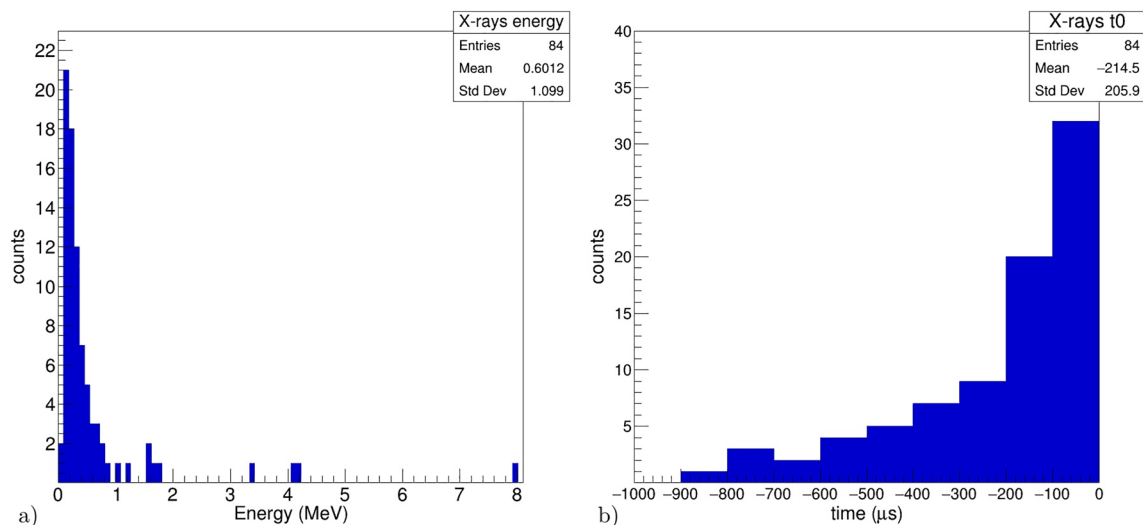


Figure 3. (a) Energy distribution of the X-ray detected during the bursts observed. The highest energy values can be real or overestimated due to a pile-up effect. The nominal time resolution to excluding pile-up is 0.5 μ s. (b) Time distribution of the X-ray pulses detected during the bursts observed in negative downward leaders before the return stroke.

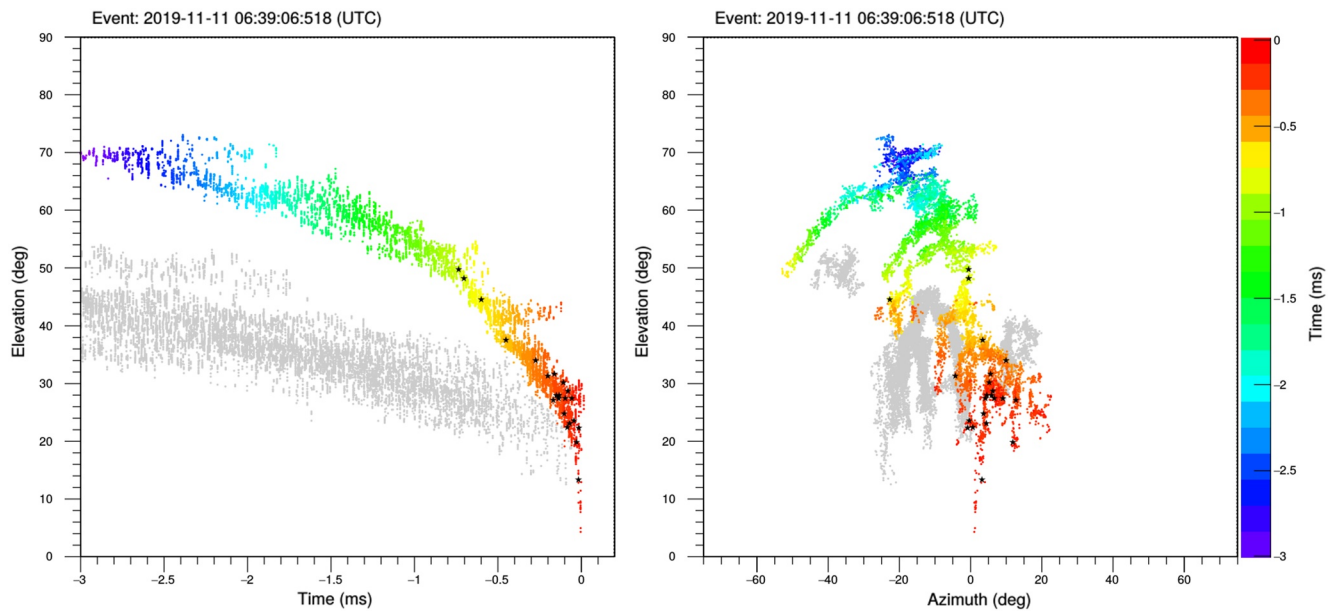


Figure 4. Negative downward leader associated with the detection of an X-ray burst. The lightning map is obtained with the VHF broadband lightning interferometer INTF-1. The image is colored by time and the most likely locations of the X-ray sources is marked with black stars. The gray image is related to another simultaneous leader branch likely farther away from the interferometer.

lightning activity. In this section, we present the most energetic burst associated with a negative downward leader and subsequently a dart leader event that occurred 4 ms later.

The first relevant observation is that all the X-ray bursts detected were associated with negative downward leaders with several branches. In particular, in this case, it is possible to distinguish two main leader branches: The first one at a lower elevation, probably farther away from the INTF or with lower speed, and the second one at a higher elevation probably closer to the INTF or faster. This ambiguity is due to the two-dimensional imaging of a three-dimensional development of a lightning event. We will focus especially on this second main leader branch because the high-energy radiation detected seems to be associated with its propagation.

Figure 4 and Figure 5 show the negative downward leader evolution during the last 3 ms before the RS. The lightning map is 2D and it is described by the angular coordinates: Elevation and azimuth defined in Section 2.1 and in Figure 1b. The timestamp in UTC time is the proper time of the RS detected by LINET. In order to better appreciate the evolution in time, especially when the X-ray emissions were detected, we provide an animation of Figure 4 in the supplementary material.

For this event, it was possible to obtain a relatively accurate location of the radial distance comparing the LINET location with pictures and satellite images of the struck area and likely this distance is 430–450 m, two high-buildings are the most likely striking point. In Figure 5 it is possible to appreciate the detailed evolution of the downward leader and the most likely location of the X-ray sources.

In order to describe the procedure by which the most likely X-ray sources were located, a few comments on the E-field signal, the X-ray signal, and VHF sources are needed.

Figure 6a shows the output signals of the flat plate antenna and the high-energy detector in the last 1 ms before the RS. The electric field increases due to the approaching of the downward leader to the ground until the dramatic drop at the RS. The high-energy detector signal shows the overlap of the X-ray pulses due to the long decay constant of the detector. This pile-up effect can be resolved for time intervals greater than $0.5 \mu\text{s}$. The time-of-arrival t_0 of each X-ray pulse was evaluated and numbered.

Figure 6b allows us to clarify the terminology used in this work. We use the term “VHF sources” to indicate the set of all solutions provided by the interferometer data processing.

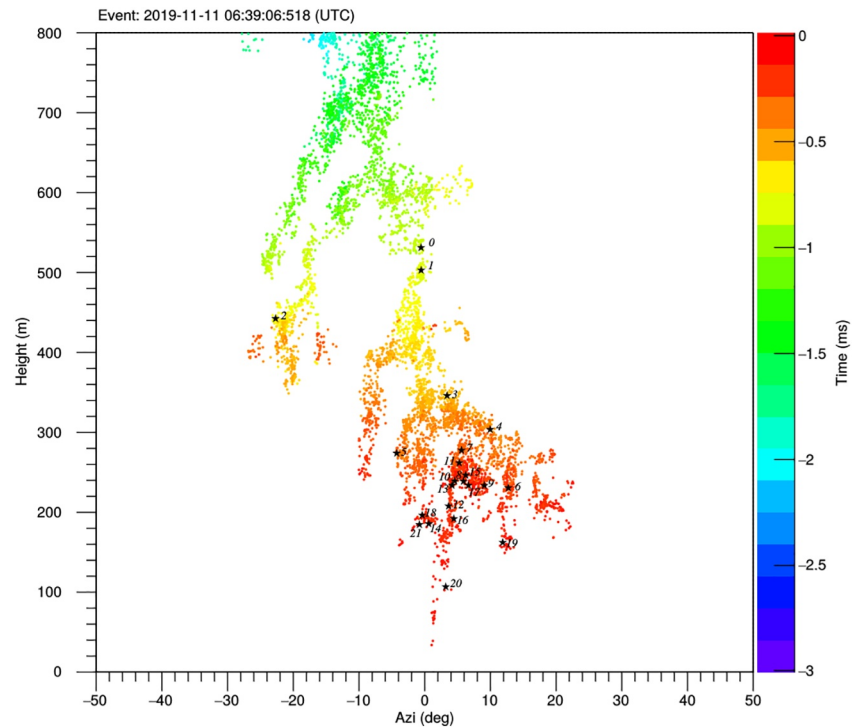


Figure 5. Negative downward leader associated with the detection of an X-ray burst. The lightning map is obtained with the VHF broadband lightning interferometer INTF-1. The image is colored by time and the most likely location of the X-ray sources is marked with black stars.

In general, the VHF sources detected by a broadband lightning interferometer can be due to continuously radiating or impulsive events (Stock et al., 2014). We are especially interested in a subset of these VHF sources that we call “the most intense VHF pulses.” We define this subset considering a local maximum

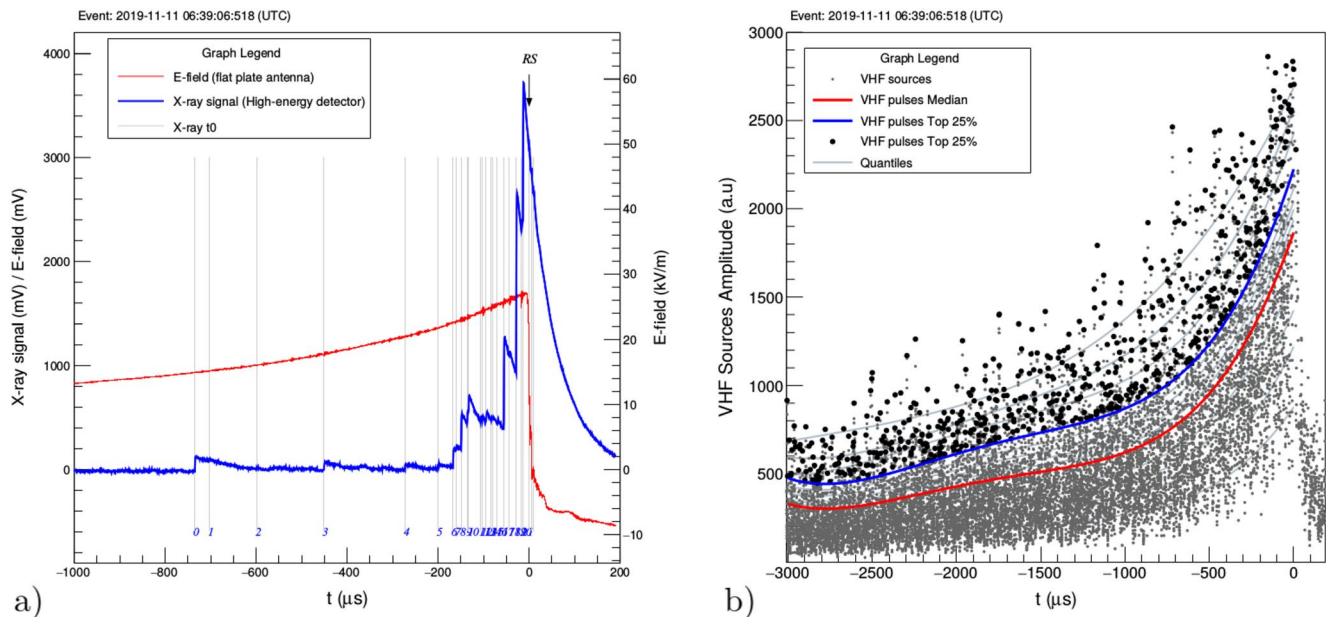


Figure 6. (a) Electric field from the flat plate antenna and high-energy detector signal in the last 1 ms before the return stroke. (b) VHF sources and VHF pulses amplitude in the last 3 ms before the return stroke. The red line and the blue line represent the VHF pulses median and the third quartile respectively, which define the most intense VHF pulses.

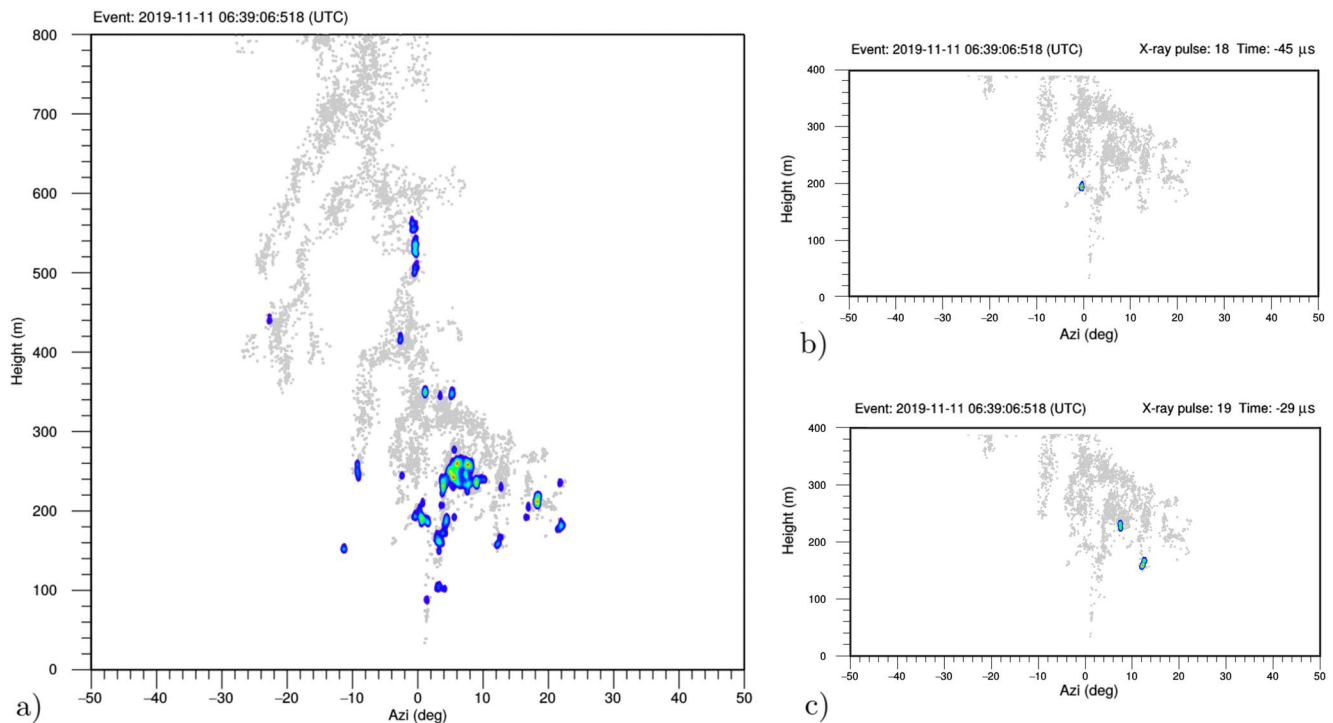


Figure 7. (a) Density plot of all the VHF sources that can be related to the high-energy emission in a time interval δt of $\pm 1 \mu s$ with respect to all X-ray t_0 . (b) Unique location of X-ray pulse 18. (c) Ambiguous location of X-ray pulse 19.

condition and a threshold condition on the VHF amplitude. The local maximum condition on the amplitude, generally defines a “VHF pulse,” instead, the threshold condition on the amplitude, based on the median or the third quartile (top 25%), allows to define in a robust way the “most intense VHF pulses.” More details are available in the Supporting Information.

With only one high-energy detector, it was not possible to obtain an independent measurement to locate the X-ray sources. Therefore, our initial assumption was to associate each X-ray t_0 with the closest VHF sources in time domain and infer the X-ray source location from the associated VHF source location. Following this procedure, we realized that several VHF sources could be associated with the same X-ray in our uncertainty range, dominated by the rise time of the high-energy detector. For this reason, in order to express this uncertainty in the location of the high-energy radiation, a good strategy consists in plot all the possible X-ray sources in a time interval δt with respect to X-ray t_0 . We have chosen $\delta t = \pm 1 \mu s$ because it is the double of our uncertainty range, and assuming a normal random distribution, it would correspond to a 95% of confidence interval.

Figure 7a shows the density plot of VHF sources in this interval; it is probably the most effective way to show all the possible locations of the X-rays detected together with their location uncertainty. Despite that, this figure is integrated over a long time compared to the single X-ray emission and it is not allowed to evaluate the location uncertainty of each X-ray pulse detect. Therefore, we provide in Figure 7 two example of the location uncertainty related to the X-ray pulses number 18 and 19 (all the other cases can be find in supplementary material). Figure 7b shows an unique location of the X-ray source, instead, Figure 7c shows an ambiguous location.

Despite this occasional ambiguity on the X-ray source location, we were not sure that the VHF emissions and the high-energy radiation were related until we observed a clear correspondence between the X-ray t_0 and the most intense VHF pulses.

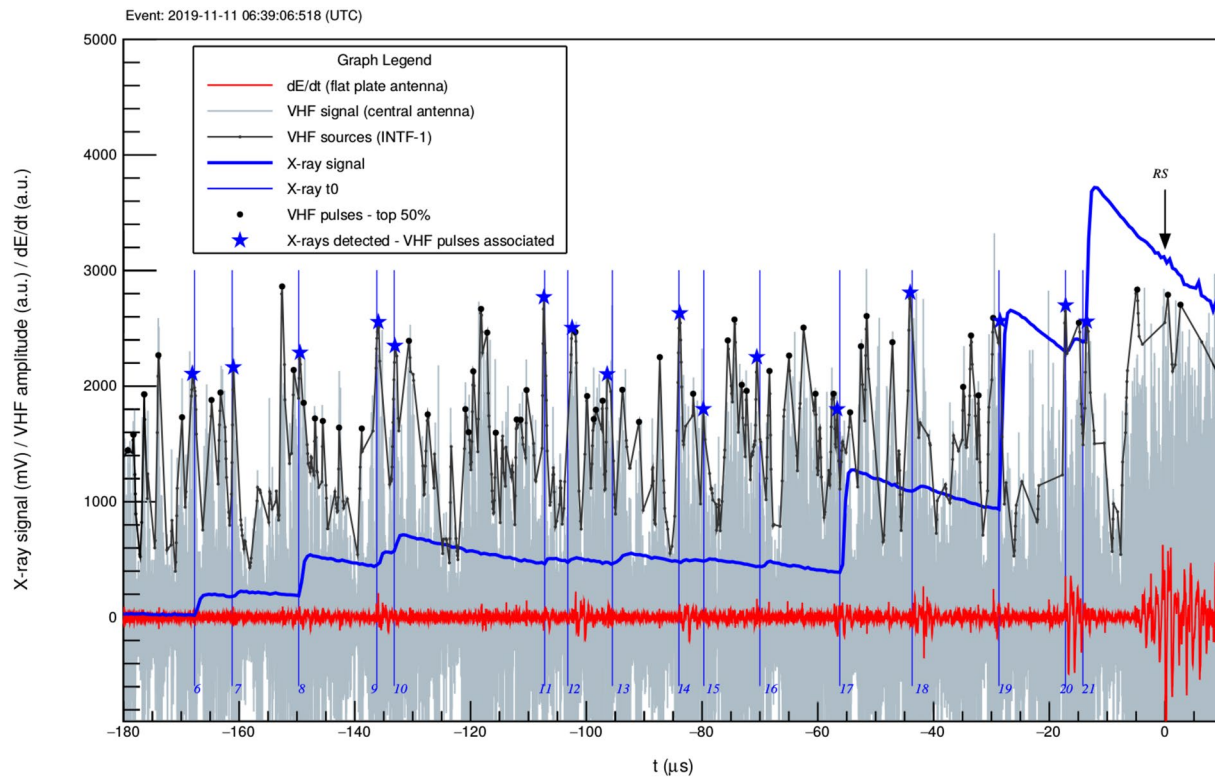


Figure 8. Zoom of the most interesting time interval of Event 2019-11-11 06:39:06. The graph highlights the temporal correspondence between the X-ray pulses (blue lines and labels) and the most intense VHF pulses (black dots and blue stars). The association is marked with blue stars.

3.2.1. Temporal Correspondence Between the High-Energy Emissions and the Most Intense VHF Pulses

In this section, we present the evidence of a temporal correspondence between the high-energy emissions and the most intense VHF pulses. We compare the time-of-arrival of the high-energy emissions t_0 , computed by the algorithm described in Section 2.2, with the time-of-arrival of the VHF emissions, computed by the interferometer. Further details on the data processing and the quantitative definition of the VHF source amplitude are described in the Supporting Information.

Figure 8 shows a clear example of this temporal correspondence. On the background, it is possible to observe the VHF signal of the central antenna (gray line). The black spline connects all the VHF sources obtained by the INTF processing and in particular, the most intense VHF pulses marked with black dots. The output signal of the high-energy detector and the dE/dt signal are respectively the blue and the red line.

It is possible to observe how the black spline presents several peaks, which correspond to the most intense VHF pulses. Superimposing a vertical reference related with t_0 (blue lines) emerges the correspondence with VHF peaks. A blue star mark represents the matching.

As already mentioned, there are several VHF sources that could be associated with the same X-ray pulse in our uncertainty range, but usually only one intense VHF pulse. Nonetheless, to prove the goodness of this correspondence, we performed two complementary analyses.

The first test consists in computing the discrete cross-correlation between the X-ray time-of-arrivals t_0 and the VHF pulses timestamps, considering the temporal uncertainty of $\pm 0.5 \mu\text{s}$ as the width of the t_0 pulses. The result shows a correlation peak compatible with zero, therefore, we can state that high-energy pulses and VHF pulses are temporally correlated. Furthermore, following a similar approach we computed the cross-correlation between the X-ray time-of-arrivals t_0 and the most intense VHF pulses (top 25%) and we compared it with the cross-correlation with the other VHF pulses (bottom 75%). Figure 9a shows that there

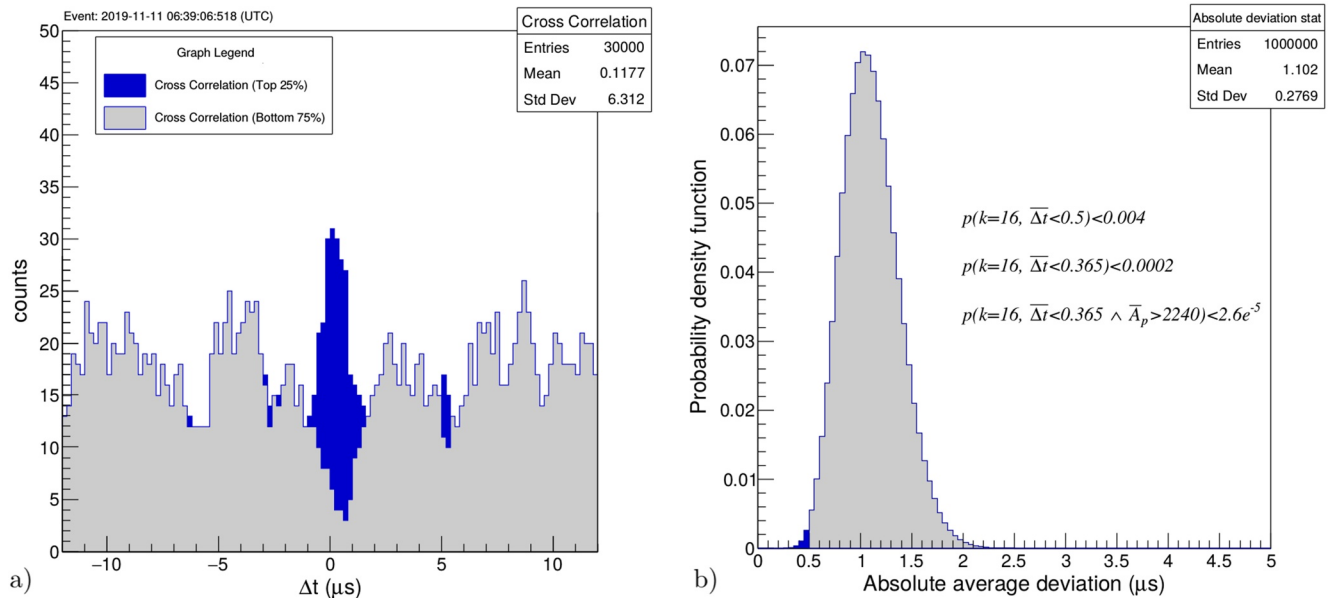


Figure 9. (a) Cross-correlation between X-ray t_0 and the most intense VHF pulses (top 25%), and between the less intense VHF pulses (bottom 75%). In both cases we considered an uncertainty of $\pm 0.5 \mu s$ on t_0 . (b) Probability density function obtained from a Monte Carlo simulation to evaluate the p-value, in the case of study presented in Figure 8.

is a clear correlation between the X-ray time-of-arrivals t_0 and the most intense VHF pulses, instead there is no correlation with VHF pulses with lower amplitude.

The second test we performed is a Monte Carlo simulation to evaluate the p-value in the case of study illustrated in Figure 8. We considered all the most intense VHF Pulses (top 50%) and we simulated the X-ray t_0^* assuming a random uniform distribution in the time range $[-180:0] \mu s$, then we evaluated the absolute deviation $\Delta t = |t_0^* - t_{VHF}|$. The probability to have a single random correspondence is actually quite high $p(k=1, \Delta t < 0.5) < 0.366$, but the probability to have several random correspondences decrease rapidly.

We evaluated the average absolute deviation for 16 correspondences. The probability density function is shown in Figure 9b. The probability for a random correspondence in the uncertainty range is less than 0.4% but the p-value of our event is lower than 0.02% and if we consider the average VHF amplitude as well, the probability to have a random association with overall higher VHF amplitude is absolutely low ($p < 2.6 \times 10^{-6}$).

After that, we evaluated the deviation $\Delta t = t_0 - t_{VHF}$ of the measured X-ray t_0 , where t_{VHF} is the time related to the VHF pulse associated. This quantity Δt was computed for all the X-ray bursts observed and shows that both processes could be considered simultaneous within an accuracy of $0.5 \mu s$ (see Figure 10a).

Despite the definition of “the most intense VHF pulses” provided is generally clear, we studied the relation with the VHF amplitude more thoroughly. We computed the 20-quantiles in all the X-ray bursts observed in order to compare the relative magnitude of the VHF amplitude of the pulses associated with the high-energy emissions.

The overall distribution is shown in Figure 10b, the most intense VHF pulses (top 50%) correspond to more than 96% and the top 25% correspond to the 82% of the distribution.

In conclusion, we can state that a temporal correspondence between the high-energy emissions and the most intense VHF pulses was observed and it is statically significant. This temporal correlation allows a more accurate location of the X-ray sources and could suggest a shared production mechanism.

It is relevant to note that also the peaks of the electric field derivative (dE/dt) are in correspondence of the X-rays pulses, as observed for the first time by Dwyer et al. (2005) and with the majority of the VHF pulses.

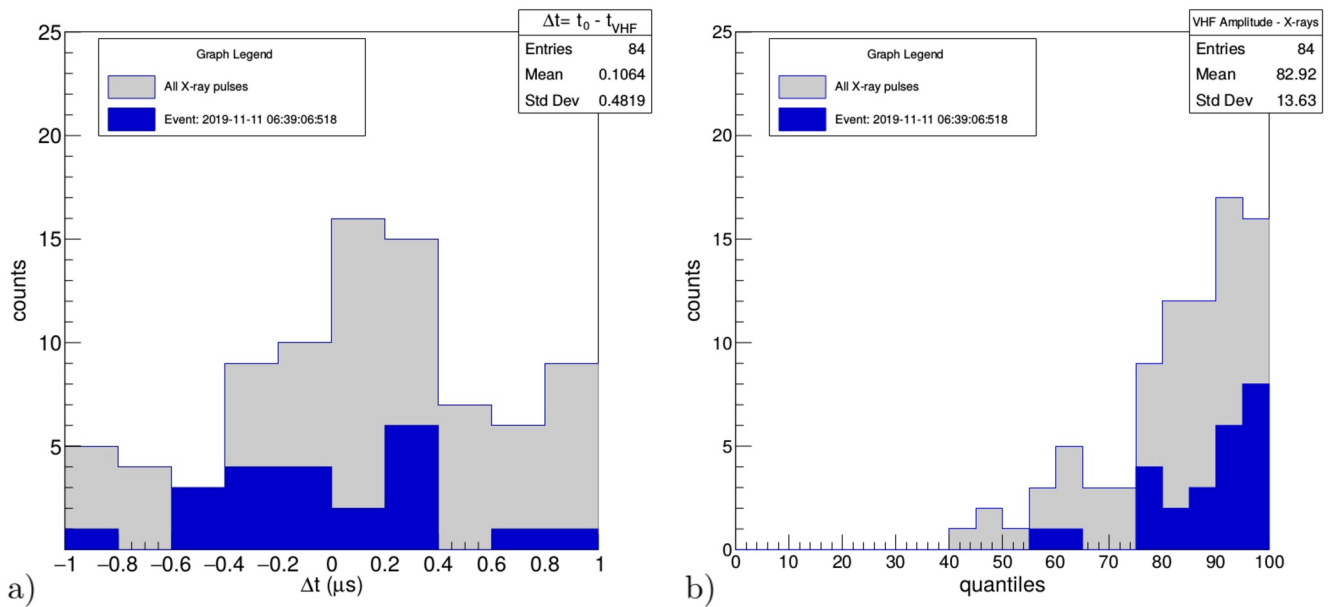


Figure 10. (a) Time difference between the X-ray t_0 and the VHF pulses associated. This quantity was evaluated in all X-ray bursts (gray) and in the X-ray burst 2019-11-11 06:39:06 (blue). (b) Distribution of the VHF pulses associated with X-ray emissions. The VHF amplitude is expressed in quantiles to allow comparison between different events.

This “triple” correlation between high-energy radiation, VHF pulses and electric field derivative dE/dt is discussed in Section 4.

3.2.2. High-Energy Emissions and Leader Speed

In this section we investigate the relation between the high-energy radiation and the VHF leader speed. The goal of these measurements is not intended to provide an accurate absolute value of the leader speed, but rather to investigate whether it is possible to observe some correlation or change in speed in correspondence with the high-energy emission. Assuming a good accuracy in the radial distance (≈ 450 m) and a leader development, essentially vertical, it is possible to quantify the 2D speed of the leader.

The attempt to calculate the speed between two consecutive VHF sources has failed, this procedure produces unreliable values of the leader speed. The reason for that could be due to the fluctuations or likely because the VHF pulses measured by the INTF are associated with the streamers’ propagation (and therefore, two consecutive streamers can be randomly directed and unrelated in terms of their propagation). To overcome this problem, we selected nine leading branches (LBs) by visually separating the VHF sources through polygons in the 2D image and then we averaged the VHF sources together in a fixed time interval of $10 \mu s$.

Figure 11 shows the 2D speed of the selected branches, the areas of great interest are delimited by a border obtained from the previous density plot. To allow better visualization, it was decided to saturate speeds above 4.0×10^6 m/s, this threshold was chosen considering the overall speed distribution.

It seems possible to observe a variation in the 2D speed in correspondence with the X-ray emissions (see the arrows in Figures 11, for example, LB2, LB3, LB5, LB8, and LB9). This speed variation can be identified by the color change, especially in the presence of red dots or warm colors, but it could also be due to multiple branching in the third dimension or in smaller scale, high streamer activity or simply random fluctuations. Therefore, although there is an indication of correspondence between the X-ray location and the 2D speed variation, such correlation is not strong enough to be statistically significant.

Despite the averaging procedure, several outliers, essentially due to fluctuations or secondary branching, compromise the measurement of the overall 2D speed of a single leader branch. For this reason, in order to get more reliable speed values for each single branch, we preferred to calculate them using an 1D linear fit

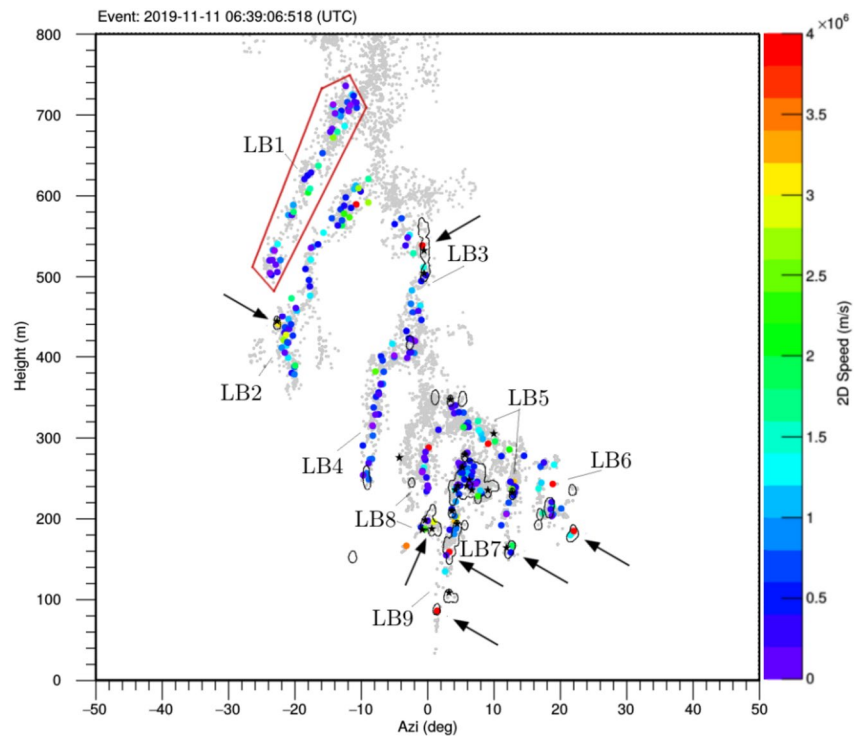


Figure 11. (a) Analysis of the leader speed in relation with the high-energy radiation. Nine leader branches were examined and the 2D speed was calculated averaging all the VHF sources in a time interval of $10 \mu\text{s}$. The regions of interest are indicated by arrows and delimited by a contour plot, the X-ray sources are marked with black stars. Speed values greater than $4.0 \times 10^6 \text{ m/s}$ were saturated to this maximum value.

(see Figure 12). We take advantage of the 2D imaging to select the branches and compute the 1D speed in both components (vertical and horizontal) and then obtain the 2D speed by combining both.

In conclusion, although we investigated the relation between the high-energy radiation and the VHF leader speed, we did not observe a clear correlation. It is possible to report that high-energy radiation was observed in negative downward leader propagation in the 2D speed range $0.4\text{--}1.2 \times 10^6 \text{ m/s}$. Further implications are discussed in Section 4.

3.3. Dart Leader: 2019-11-11 06:39:06

After 4 ms from the previous negative downward leaders, we observed dart leader event with X-ray emissions. In Figure 13, it is possible to appreciate the development of the dart leader along the main channel of the previous event (in gray). Two X-ray pulses were observed in coincidence, both with an energy of about 100 keV. The total duration of the event is about $100 \mu\text{s}$.

Figure 14 shows the vertical evolution of the dart leader during the last $50 \mu\text{s}$ before the return stroke. We used linear interpolation to calculate the 1D speed in both components (vertical and horizontal) to determine the 2D speed. The average speed seems constant for the last 800 m with a value of $2.0 \times 10^7 \text{ m/s}$. We did not observe measurable increase of the speed in the proximity of the X-ray emissions. A strong VHF signature was observed, typical of dart leaders. The elapsed time between the VHF pulses is much less than the negative downward leaders. Further implications are discussed in Section 4.

3.4. Negative Downward Leaders: 2019-11-11 06:38:16

A similar analysis to the one described for the event 2019-11-11 06:39:06 is conducted on all observed X-ray bursts, but in less detail due to the larger uncertainty on the distance and a smaller number of X-rays

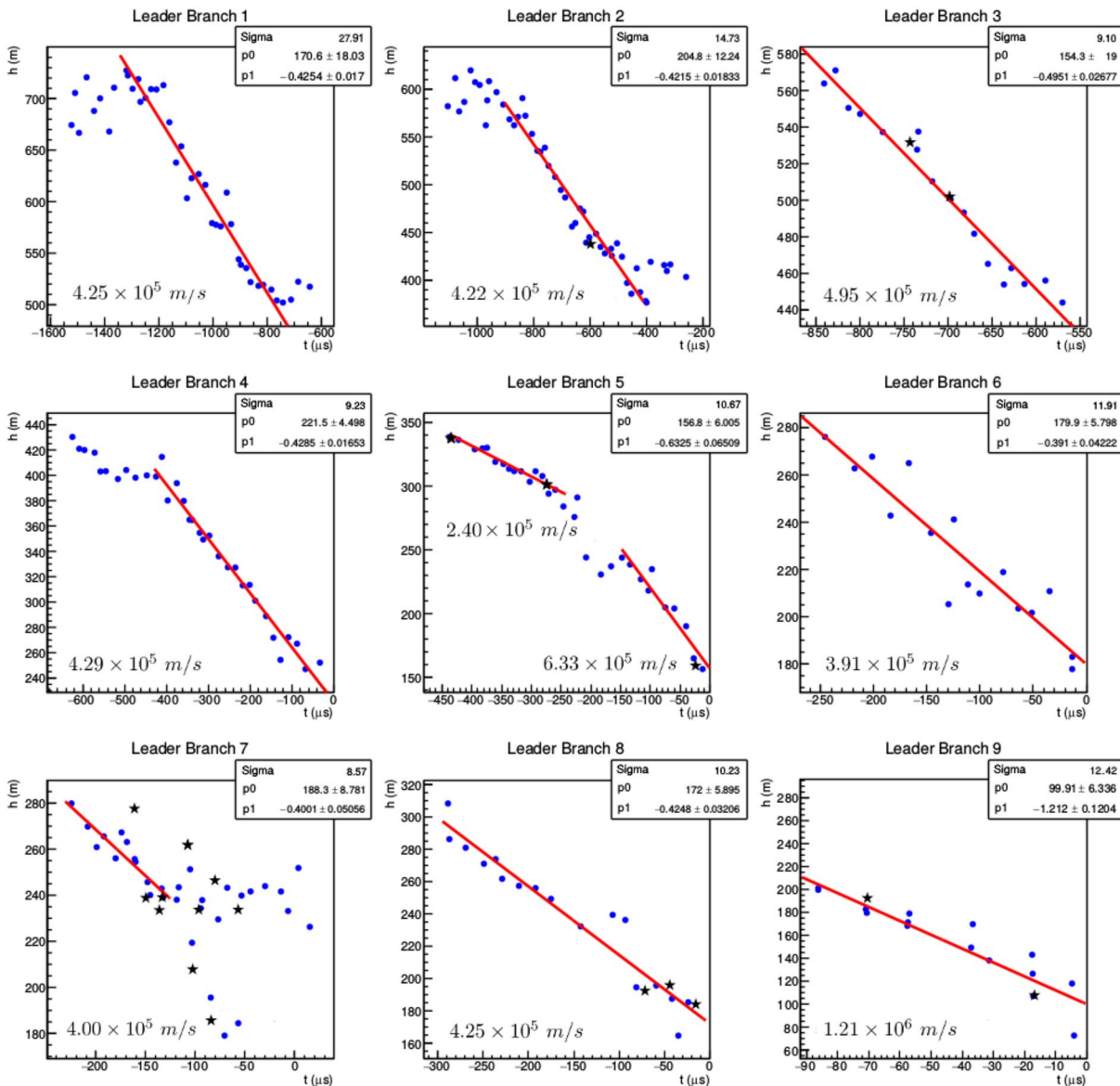


Figure 12. Collection of nine leader branches of the lightning event 2019-11-11 06:39:06:518 (UTC). The graphs show the VHF sources averaged in a time interval of $10 \mu\text{s}$. The height-time plot shows the 1D averaged leader speed computing the slope ($p1$) of the linear fit. It is possible to appreciate the variation of the leader speed and secondary branching in the time domain. The likely sources of high-energy radiation are marked with black stars.

detected. For completeness and further considerations, we briefly present another case of negative downward leaders: 2019-11-11 06:38:16.

Figure 15a shows the location of the high-energy sources with their uncertainty expressed by the density plot. This case is characterized by three simultaneous distinct leaders' main branches all around our INTF station (note azimuth scale). The duration of the X-ray burst is about 1 ms with 23 X-ray single pulses detected. We observed many X-ray sources in correspondence with the unconnected leader tips.

LINET provides a unique location for this event (likely related to LB4 the channel where the return stroke occurred), the approximate distance from the INTF station is 550 m. Assuming this value for all the LBs, we calculated the 2D speed: $0.8\text{--}1.0 \times 10^6 \text{ m/s}$ for LB1, LB2, LB3, and $1.2 \times 10^6 \text{ m/s}$ for LB4.

As a final remark, we would like to point out that an X-ray burst can have multiple sources belonging to different leader branches, that could be hundreds of meters apart. Therefore, an extensive origin of the X-ray

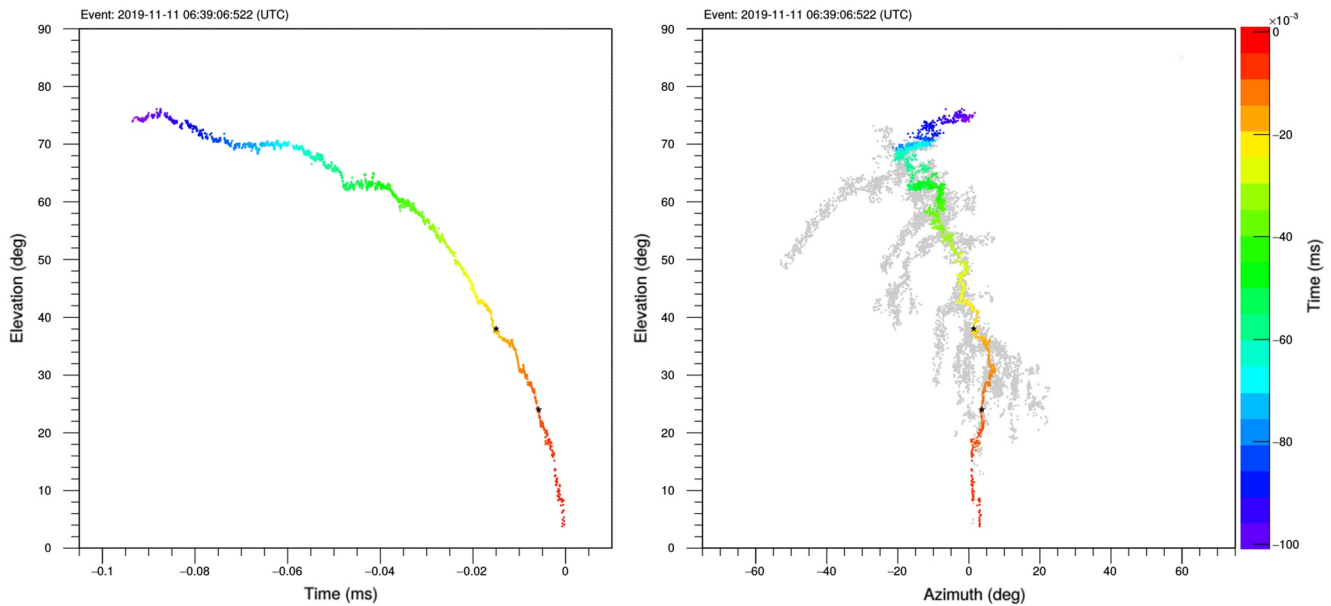


Figure 13. Dart leader associated with the detection of high-energy emissions. The lightning map is obtained with the VHF broadband lightning interferometer (INTF-1). The image is colored by time and the most likely location of the X-ray sources is marked with black stars.

burst should be considered, the same also in downward TGFs like those observed by Abbasi et al. (2019) and maybe, we hypothesize, in TGFs detected from space.

4. Discussion

In this study, we presented simultaneous measurements of high-energy radiation and lightning imaging provided by a VHF broadband interferometer. In comparison with other studies, the main advantage of this approach is to observe directly the lightning leaders propagation and measure in coincidence the high-energy radiation with sub-microsecond time accuracy. On the other hand, the main limitations of our setup are related to the use of a single high-energy detector and the partial information provided by the 2D imaging of the interferometer.

As previously discussed in Section 3.1, a single detector does not allow to obtain an independent measurement to spatially locate the high-energy sources, while in other studies (Hill, 2012; Howard et al., 2008), it was possible to locate the high-energy sources directly using several detectors in 3D via TOA techniques.

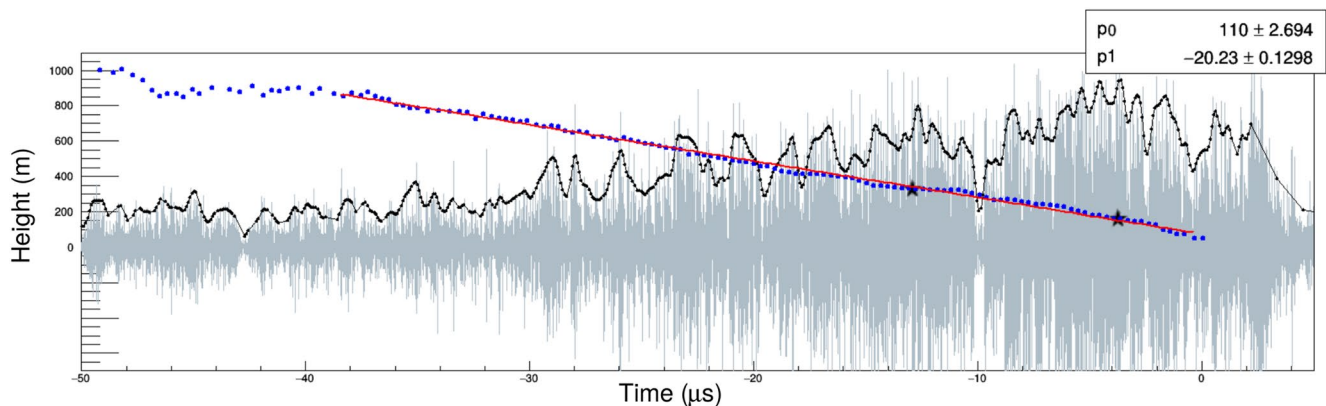


Figure 14. Analysis of the 1D-speed of the dart leader. The graph shows in background the VHF signal and in black dot line the VHF amplitude of the sources. The time evolution of the VHF source height is depicted with blue dots and the black star markers represent the most likely height of the X-ray sources. Finally, the linear interpolation of the speed is superimposed.

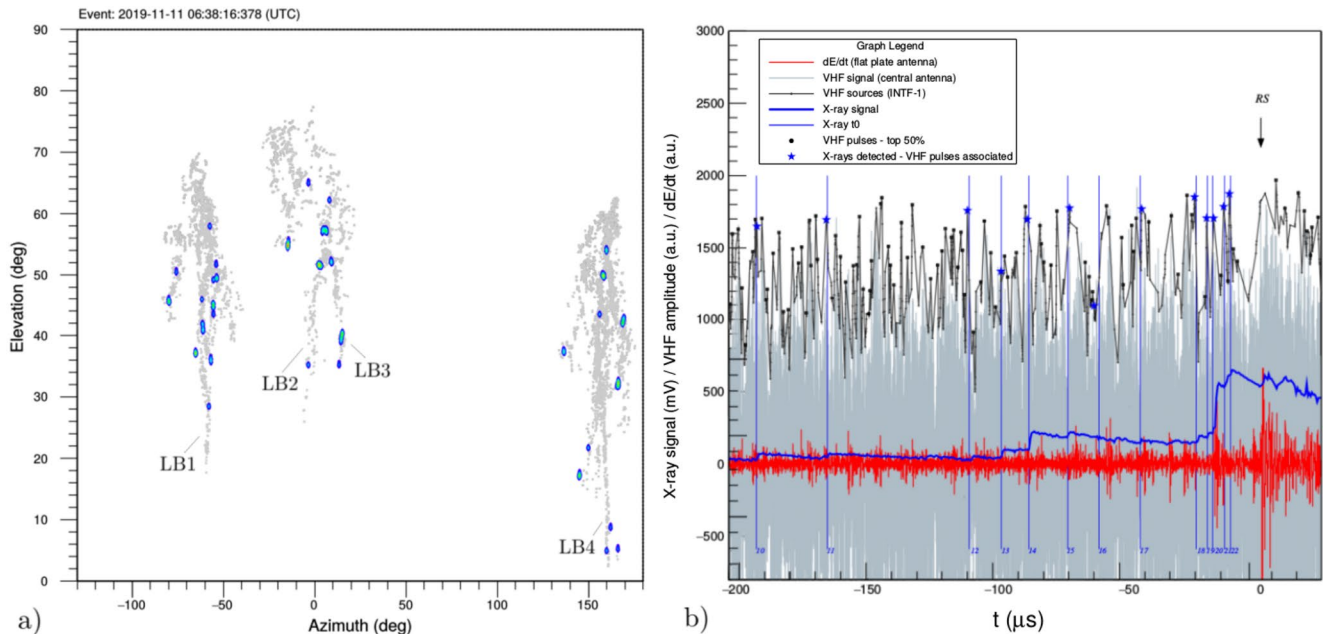


Figure 15. Negative downward leaders event associated with the detection of an X-ray burst. (a) Density plot of all the VHF sources that could be related to the high-energy emission in a time interval δt of $\pm 1 \mu s$ with respect to the X-ray t_0 . (b) Temporal association between the X-ray pulses (blue lines and labels) and VHF amplitude peaks, the correspondence is marked with blue stars. Zoom of the last $200 \mu s$.

Despite this limitation, we observed a strong temporal correspondence between the X-ray detection and the most intense VHF pulses that can be used to locate the VHF sources associated with the high-energy radiation. The time difference between the X-ray detection and the VHF pulses is shown in Figure 10a and suggests the simultaneity of the two processes within a time interval comparable with our instrumental uncertainty $0.5 \mu s$. A similar time correspondence, between the high-energy radiation and the electric field derivative dE/dt , had already been observed by Dwyer et al. (2005) and associated with the leader step process. Howard et al. (2008) studied the co-location between the electric field change sources and the high-energy emissions. They observed that X-rays are emitted $0.1\text{--}1.3 \mu s$ after the dE/dt pulses at an average distance of 50 m. Instead, our observations show the location of the VHF sources (associated with the high-energy radiation) and not directly the high-energy sources.

The other significant limitation is due to the 2D imaging of the interferometer. In particular, two consequences derive from it: The lack of information on the distance of the source, which cannot be obtained directly from our measurements, and the lack of information on the spatial direction of the leader branches. Without knowing the distance of the sources, it is not possible to estimate correctly the leader speed and the intensity of the high-energy sources. In addition, without knowing the direction of the leader branches, it is difficult to consider and discuss the beaming effect due to the orientation of the leaders. In order to overcome these limitations, we installed two interferometers (INTF-1 and INTF-2) for a limited period of time, but unfortunately, we did not observe any X-ray burst in coincidence with both interferometers. Therefore, we used LINET data to obtain the complementary information for our measurements, in particular the distance between the event and INTF-1 and the stroke peak current.

In spite of the limitations discussed, the images obtained with the VHF broadband interferometer allow to appreciate in detail the leader's development and to locate with good accuracy the VHF sources associated with the high-energy radiation. The bottleneck of our accuracy is due to the rise time $\sim 0.5 \mu s$ of the high-energy detector and secondarily the digitizer sampling rate. As explained in Section 3.2, it is not particularly relevant to estimate the spatial accuracy of the high-energy sources location in terms of meter or degrees because in our temporal uncertainty multiple VHF sources can be associated with the same X-ray. For this reason, we selected the most intense VHF pulses in the interval δt of $\pm 1 \mu s$ and we represented our uncertainty in the density scatter plot (Figures 7a and 15a). Despite the discussed uncertainty, there is clear

evidence from our data that the high-energy radiation sources detected during negative downward leaders propagation can be associated with different leader branches (Figures 7b–7c and 15a). We have tried to catalog the locations of high energy sources in a possible relevant position during the propagation of the leaders (branching point, end of the unconnected leader channel, change of direction, change of speed, final jump) with respect to random leader steps, but we cannot state any clear conclusion. Although most of them, in particular the end of an unconnected leader channel (~23%) and the branching point (~12%) seem to be more frequent than a random leader step.

Even if, as already discussed, we are not able to reconstruct in 3D the direction of the leader channels, there are two observations in favor of the thesis that the high-energy radiation flux is beamed forward as observed in particular by Howard et al. (2010), Montanyà et al. (2014) and Saba et al. (2019). The first observation is related to the LB7 in Figure 12. It is possible to realize that the evident branching in time domain on a narrow selection ($\Delta Az_i < 5^\circ$) correspond to a branching in the direction of the INTF and probably this justifies the unusual high number of high-energy sources detected in the same location.

The second observation is related to the dart leader case. There are numerous evidence that dart leaders radiate high-energy radiation and according to Mallick et al. (2012) in subsequent strokes the chance to detect X-ray is higher. In contrast, we detected only two low energetic X-ray pulses with an energy of about 100 keV, probably due to secondary Compton scattering. This observation is consistent with Saba et al. (2019) measurements, which confirm the important role of the leader orientation in the X-ray detection.

At the end of Section 3.2, we have already discussed the methodology to compute the 1D and 2D leader speed and the difficulties related to their measurement. The results obtained are in a very good agreement in particular with the work of Howard et al. (2010), where high-energy radiation was detected in natural CG lightning with a leader speed range of $3.6\text{--}9.0 \times 10^5$ m/s and with Tran and Rakov (2017), who reported a leader speed range approaching to the ground of $1.8\text{--}6.0 \times 10^5$ m/s.

Finally, we believe that the association between X-ray emissions and strong VHF pulses could be a key element in the study and understanding of high-energy emission phenomena. This association, in fact, reveals that both RF emissions and high-energy radiation likely share a production mechanism (Howard et al., 2008; Montanyà et al., 2015; Tierney et al., 2005).

The results presented and discussed have some relevant implications: On the origin of the intense VHF pulses, on the origin of the high-energy radiation, and in particular, on the origin of the TGFs.

4.1. Implications on the Origin of the Most Intense VHF Pulses

A recent study has established that VHF emissions from stepping negative leaders in lightning is most likely due to streamer formation around the region of the step (Hare et al., 2020). It is interesting to note that observations in laboratory experiments (Kochkin et al., 2014; Montanyà et al., 2015), models (Gurevich et al., 2007) and simulations (Celestin & Pasko, 2011; Chanrion & Neubert, 2010) agree that the high-energy radiation is associated with streamers development and in particular, the tip of the streamer provides the high electric field needed to initiate the electron runaway.

Therefore, the association between high-energy radiation and VHF pulses observed suggests that the origin of the VHF pulses could be due to the runaway electrons mechanism, or more in general, to the high-energy electron acceleration. It is well known that accelerated electrons produce an intense electromagnetic radiation field, whose emitted power is proportional to the square of the acceleration according to the Larmor formula. It is possible to show that the radiation spectrum in frequency domain justifies the VHF signature observed. In particular, it is relevant to note that the emitted power increases drastically in the relativistic regime.

A very high field cannot exist in air for very long, since conventional breakdown will rapidly discharge the field (Dwyer & Uman, 2014). The consequence of this fact is that the runaway electrons mechanism in lightning discharges is an impulsive phenomenon. In summary, high-energy radiation and the most intense VHF emissions likely share the runaway electrons as a common production mechanism. This could explain in particular, the intensity and impulsive nature observed in the VHF bandwidth.

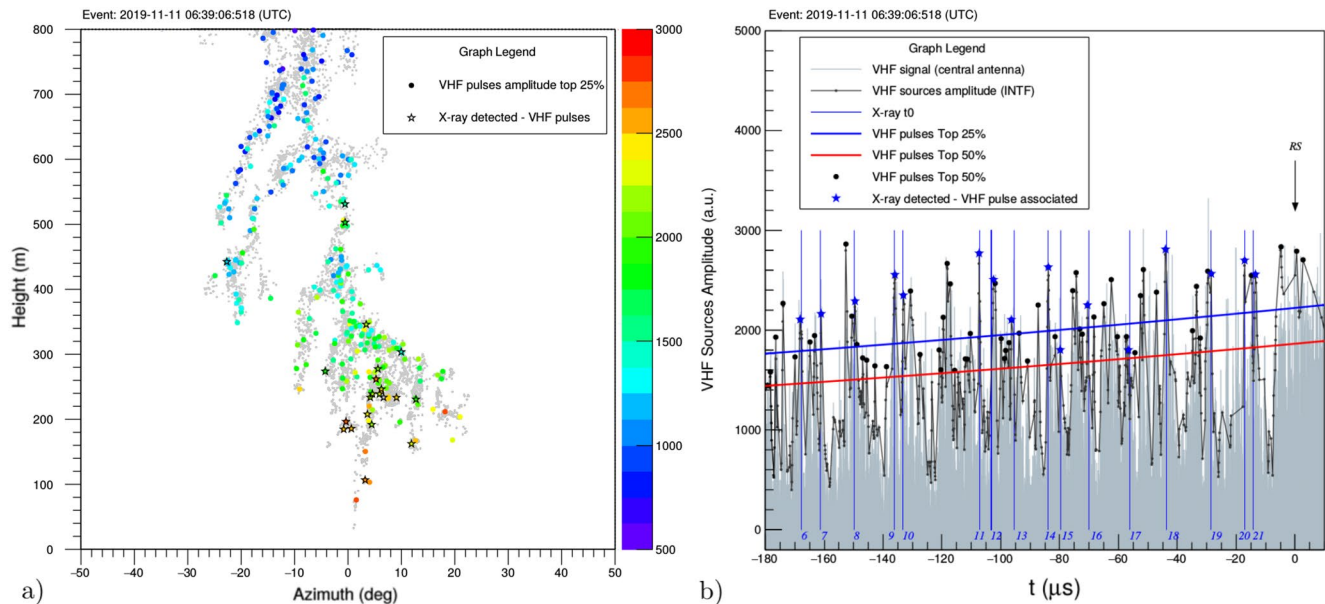


Figure 16. Assumption of a correspondence between the most intense VHF pulses and the high-energy radiation sources applied on real data. (a) Most intense VHF sources, colored by VHF amplitude, if associated with X-ray detection marked with black stars. (b) Temporal correspondence between VHF pulses and high-energy radiation sources. If the correspondence was really observed (blue stars) if only hypothesized (black dots).

4.2. Implications on the Origin of the High-Energy Radiation

High-energy radiation undergoes a strong absorption exponentially proportional to the density of the air (e.g., Hubbell & Seltzer, 1995) which plays a crucial role in the detection, especially in ground-based observations. The strong absorption explains why the X-ray detection from lightning requires to be very close to the lightning discharge as shown by the results obtained in Section 3.1. Furthermore, the small effective detector area ($\sim 0.02 \text{ m}^2$) considerably limits the chance of observation. Based on these considerations, it is reasonable to think that observed X-rays are a very small fraction compared to those actually produced by lightning leaders. This conclusion is in agreement with Monte Carlo simulations and absorption models (Berge & Celestin, 2019; Celestin et al., 2015; Østgaard et al., 2008).

In Figure 16, we considered the negative downward leaders event described in detail in Section 3.2 and we hypothesized that all the most intense VHF pulses are associated with sources of high-energy radiation. Assuming that, the number of high-energy radiation sources is potentially greater than the one observed, many more sources ($\approx 10^2 - 10^3$) have to be taken into account.

Clearly, high-energy radiation requires energetic electrons and a threshold has to be considered to assume the correspondence with the VHF pulses, but if we assume that runaway electrons is the shared mechanism, the amplitude of the VHF pulses is related to electrons acceleration, hence it can be considered a good criterion to infer the high-energy production.

Therefore, with reference to Figure 16b, if an X-ray detection is associated with a VHF pulse, there is no reason to think that another VHF pulse with comparable amplitude cannot be considered as a source of high-energy radiation too.

In our measurements, high-energy radiation has been detected in negative downward leaders with a 2D speed range of $0.4 - 1.2 \times 10^6 \text{ m/s}$ and in a dart leader with a 2D speed of $2.0 \times 10^7 \text{ m/s}$. Unfortunately, we were not able to establish a strong relation between the leader speeds required for high-energy production, although we speculate that intense VHF pulses in negative leader with comparable speed could be considered as high-energy sources.

4.3. Implications on the Origin of the TGFs

Although our measurements are related to high-energy radiation in cloud-to-ground lightning, some relevant considerations could be extrapolated for TGFs detected from the space. First of all, it is evident from our analysis that the X-ray bursts detected in coincidence with negative downward leaders are originated by multiple sources of high-energy radiation. As discussed in the previous section, the number of these sources is clearly underestimated by ground measurements, essentially due to the strong absorption exponentially proportional to air density.

This suggests that the origin of TGFs could be seen as the cumulative effect of many sources, each capable of generating runaway electrons. The cumulative effect is capable of explaining the origin of TGFs observed with the duration of several microseconds (e.g., $\gtrsim 50 \mu\text{s}$). This is more consistent for events with longer duration. On the other hand, in shorter TGFs, since there are fewer sources in the time interval, it is not possible to state this conclusion with the same confidence. This hypothesis supported by our observations is in agreement with Celestin and Pasko (2012) simulations and Dwyer and Cummer (2013) calculations. From a spatial point of view, the multiplicity of sources translates into an extensive origin of the TGF radiation.

The association between X-ray emission and strong VHF pulses can be considered a valuable method to locate the high-energy radiation phenomena. Furthermore, it can be a crucial criterion to locate the origin of the TGFs, as recently shown in Lyu et al. (2018) two TGFs were associated with $10 \mu\text{s}$ accuracy with a strong VHF emission detected by the Lightning Mapping Array (LMA). Our measurements can suggest that likely those strong VHF emissions can be properly associated with the high-energy radiation and therefore, that could be the most accurate spatial and temporal reference of the TGFs origin.

Moreover, it is interesting to point out a very good agreement between the leader speed measured in CG negative downward leaders and a few measurements in the literature of leader speed in IC negative upward leaders associated with TGF production. In particular, the leader speed measured by Shao et al. (2010) $0.4\text{--}0.6 \times 10^6 \text{ m/s}$ and Cummer et al. (2015), p. $0.8\text{--}1.0 \times 10^6 \text{ m/s}$. Although more investigations are needed to evaluate the relation between leader speed and high-energy radiation, leader speed could be another relevant observable in TGF studies from ground measurements.

Finally, we would like to compare our results with the downward TGFs observed by the Telescope Array reported by Abbasi et al. (2019) since their instrument allows unique ground measurements of the high-energy radiation from lightning discharges. We point out several analogies which their results (summarized in Section 1.) that allow us to believe that the observed phenomena are substantially the same.

5. Conclusions

In this work, we presented the first simultaneous X-ray measurements from natural lightning in coincidence with a VHF broadband interferometer. We can summarize the results we obtained with the following observational evidence:

- (1) Multiple high-energy radiation sources were observed and located during the propagation of negative downward leaders, in different leader branches
- (2) A strong temporal correspondence has been observed between the high-energy radiation and the most intense VHF pulses, comparable with our instrumental uncertainty $\sim 0.5 \mu\text{s}$
- (3) High-energy radiation has been detected in negative downward leaders with a 2D speed range of $0.4\text{--}1.2 \times 10^6 \text{ m/s}$ and in a dart leader with a 2D speed of $2.0 \times 10^7 \text{ m/s}$

From these observations, we have identified some relevant implications and consequences:

- (1) High-energy radiation and strong VHF pulses likely share the runaway electrons as a common production mechanism. The impulsive nature of the VHF pulses and their power are explained by the radiation field and the Larmor formula in the VHF bandwidth.
- (2) The strong absorption, exponentially proportional to the density of the air, plays a crucial role in high-energy detection, especially in ground-based observations. X-ray bursts detected in coincidence with negative downward leaders are originated by multiple sources of high-energy radiation that can

be located in the proximity of the leader step region, many more sources ($\approx 10^2 - 10^3$) can be inferred observing the most intense VHF pulses.

- (3) Assuming that TGFs are produced during the upward leaders propagation, not a unique origin has to be searched but an extensive origin due to the multiplicity of sources. Dwyer and Cummer (2013) address and put limits on this multiplicity in TGFs. This cumulative effect is able to explain the origin of TGFs observed with a duration of several microseconds.
- (4) Our measurements suggest that strong VHF emissions, like those observed by Lyu et al. (2018) with LMA, can be properly associated with the high-energy radiation and therefore that could be the most accurate spatial and temporal reference of the TGFs origin.
- (5) The results are consistent with the observations of Abbasi et al. (2019). We believe that our conclusions can find further confirmation in their future studies allowing a better understanding of the mechanisms of TGF production.

Data Availability Statement

Measurements and data file supporting the conclusions are available at: <https://doi.org/10.7910/DVN/VBOJBV>.

Acknowledgments

This project has received funding from the European Union's Horizon 2020 research and innovation program under the Marie Skłodowska-Curie grant agreement 722337. This work was supported by research grants from the Spanish Ministry of Economy and the European Regional Development Fund (FEDER): ESP2015-69909-C5-5-R and ESP2017-86263-C4-2-R and PID2019-109269RB-C42. The authors are grateful to Keraunos (Colombia) for providing LINET data. The authors would like to thank Edison Soto and Marleny Carrillo García of Universidad Industrial de Santander (UIS) for their support and availability during the observational campaign and Juan Pablo Sandoval Mejía for the maintenance of the instrumentation.

References

- Abbasi, R., Abe, M., Abu-Zayyad, T., Allen, M., Anderson, R., Azuma, R., et al. (2017). The bursts of high energy events observed by the telescope array surface detector. *Physics Letters A*, 381(32), 2565–2572.
- Abbasi, R., Abu-Zayyad, T., Allen, M., Barcikowski, E., Belz, J., Bergman, D., et al. (2018). Gamma ray showers observed at ground level in coincidence with downward lightning leaders. *Journal of Geophysical Research: Atmosphere*, 123(13), 6864–6879.
- Abbasi, R., Belz, J., Le Von, R., Rodeheffer, D., Krehbiel, P., Remington, J., & Rison, W. (2019). *Epj Web of Conferences* (Vol. 197, p. 03002). Ground-based observations of terrestrial gamma ray flashes associated with downward-directed lightning leaders. <https://doi.org/10.1051/epjconf/201919703002>
- Arabshahi, S., Dwyer, J., Cramer, E., Grove, J., Gwon, C., Hill, J., et al. (2015). The energy spectrum of X-rays from rocket-triggered lightning. *Journal of Geophysical Research: Atmosphere*, 120(20), 10–951. <https://doi.org/10.1002/2015jd023217>
- Aranguren, D., González, J., Cruz, A., Inampúés, J., Torres, H., & Pérez-Tobón, P. S. (2017). Lightning strikes on power transmission lines and lightning detection in colombia. In *2017 international symposium on lightning protection (xiv sipda)* (pp. 273–278).
- Berge, N., & Celestin, S. (2019). Constraining downward terrestrial gamma ray flashes using ground-based particle detector Arrays. *Geophysical Research Letters*, 46(14), 8424–8430. <https://doi.org/10.1029/2019gl083252>
- Betz, H. D., Schmidt, K., Laroche, P., Blanchet, P., Oettinger, W. P., Defer, E., et al. (2009). Linet—an international lightning detection network in europe. *Atmospheric Research*, 91(2–4), 564–573. <https://doi.org/10.1016/j.atmosres.2008.06.012>
- Bolic, M., Drndarevic, V., & Gueaieb, W. (2009). Pileup correction algorithms for very-high-count-rate gamma-ray spectrometry with nai (ti) detectors. *IEEE Transactions on Instrumentation and Measurement*, 59(1), 122–130.
- Carlson, B., Lehtinen, N. G., & Inan, U. S. (2009). Terrestrial gamma ray flash production by lightning current pulses. *Journal of Geophysical Research*, 114(A12). <https://doi.org/10.1029/2009ja014531>
- Celestin, S., & Pasko, V. P. (2011). Energy and fluxes of thermal runaway electrons produced by exponential growth of streamers during the stepping of lightning leaders and in transient luminous events. *Journal of Geophysical Research*, 116(A3). <https://doi.org/10.1029/2010ja016260>
- Celestin, S., & Pasko, V. P. (2012). Compton scattering effects on the duration of terrestrial gamma-ray flashes. *Geophysical Research Letters*, 39(2). <https://doi.org/10.1029/2011gl050342>
- Celestin, S., Xu, W., & Pasko, V. P. (2015). Variability in fluence and spectrum of high-energy photon bursts produced by lightning leaders. *Journal of Geophysical Research: Space Physics*, 120(12), 10–712. <https://doi.org/10.1002/2015ja021410>
- Chanrion, O., & Neubert, T. (2010). Production of runaway electrons by negative streamer discharges. *Journal of Geophysical Research*, 115(A6). <https://doi.org/10.1029/2009ja014774>
- Cummer, S. A., Lyu, F., Briggs, M. S., Fitzpatrick, G., Roberts, O. J., & Dwyer, J. R. (2015). Lightning leader altitude progression in terrestrial gamma-ray flashes. *Geophysical Research Letters*, 42(18), 7792–7798. <https://doi.org/10.1002/2015gl065228>
- Cummer, S. A., Zhai, Y., Hu, W., Smith, D. M., Lopez, L. I., & Stanley, M. A. (2005). Measurements and implications of the relationship between lightning and terrestrial gamma ray flashes. *Geophysical Research Letters*, 32(8). <https://doi.org/10.1029/2005gl022778>
- Dwyer, J. R. (2003). A fundamental limit on electric fields in air. *Geophysical Research Letters*, 30(20). <https://doi.org/10.1029/2003gl017781>
- Dwyer, J. R. (2004). Implications of x-ray emission from lightning. *Geophysical Research Letters*, 31(12). <https://doi.org/10.1029/2004gl019795>
- Dwyer, J. R. (2008). Source mechanisms of terrestrial gamma-ray flashes. *Journal of Geophysical Research*, 113(D10). <https://doi.org/10.1029/2007jd009248>
- Dwyer, J. R. (2020). Modeling Terrestrial Gamma-Ray Flashes Observed by Asim. In *EGU General Assembly Conference Abstracts* (p. 19320).
- Dwyer, J. R., & Cummer, S. A. (2013). Radio emissions from terrestrial gamma-ray flashes. *Journal of Geophysical Research Space Physics*, 118(6), 3769–3790. <https://doi.org/10.1002/jgra.50188>
- Dwyer, J. R., Rassoul, H., Al-Dayeh, M., Caraway, L., Wright, B., Chrest, A., et al. (2004). A ground level gamma-ray burst observed in association with rocket-triggered lightning. *Geophysical Research Letters*, 31(5). <https://doi.org/10.1029/2003gl018771>

- Dwyer, J. R., Rassoul, H. K., Al-Dayeh, M., Caraway, L., Chrest, A., Wright, B., et al. (2005). X-ray bursts associated with leader steps in cloud-to-ground lightning. *Geophysical Research Letters*, *32*(1). <https://doi.org/10.1029/2004gl021782>
- Dwyer, J. R., Schaal, M., Cramer, E., Arabshahi, S., Liu, N., Rassoul, H., et al. (2012). Observation of a gamma-ray flash at ground level in association with a cloud-to-ground lightning return stroke. *Journal of Geophysical Research*, *117*(A10). <https://doi.org/10.1029/2012ja017810>
- Dwyer, J. R., & Smith, D. M. (2005). A comparison between monte carlo simulations of runaway breakdown and terrestrial gamma-ray flash observations. *Geophysical Research Letters*, *32*(22). <https://doi.org/10.1029/2005gl023848>
- Dwyer, J. R., Smith, D. M., & Cummer, S. A. (2012). High-energy atmospheric physics: Terrestrial gamma-ray flashes and related phenomena. *Space Science Reviews*, *173*(1–4), 133–196. <https://doi.org/10.1007/s11214-012-9894-0>
- Dwyer, J. R., & Uman, M. A. (2014). The physics of lightning. *Physics Reports*, *534*(4), 147–241. <https://doi.org/10.1016/j.physrep.2013.09.004>
- Fishman, G. J., Bhat, P. N., Mallozzi, R., Horack, J. M., Koshut, T., Kouveliotou, C., et al. (1994). Discovery of intense gamma-ray flashes of atmospheric origin. *Science*, *264*(5163), 1313–1316. <https://doi.org/10.1126/science.264.5163.1313>
- Gurevich, A., Milikh, G., & Roussel-Dupre, R. (1992). Runaway electron mechanism of air breakdown and preconditioning during a thunderstorm. *Physics Letters A*, *165*(5–6), 463–468. [https://doi.org/10.1016/0375-9601\(92\)90348-p](https://doi.org/10.1016/0375-9601(92)90348-p)
- Gurevich, A., Zybin, K., & Medvedev, Y. V. (2007). Runaway breakdown in strong electric field as a source of terrestrial gamma flashes and gamma bursts in lightning leader steps. *Physics Letters A*, *361*(1–2), 119–125. <https://doi.org/10.1016/j.physleta.2006.05.063>
- Hare, B. M., Scholten, O., Dwyer, J., Ebert, U., Nijdam, S., Bonardi, A., et al. (2020). Radio emission reveals inner meter-scale structure of negative lightning leader steps. *Physical Review Letters*, *124*, 105101. <https://doi.org/10.1103/PhysRevLett.124.105101>
- Hare, B. M., Uman, M. A., Dwyer, J. R., Jordan, D. M., Biggerstaff, M. I., Caicedo, J. A., et al. (2016). Ground-level observation of a terrestrial gamma ray flash initiated by a triggered lightning. *Journal of Geophysical Research - D: Atmospheres*, *121*(11), 6511–6533. <https://doi.org/10.1002/2015jd024426>
- Hettiarachchi, P., Cooray, V., Diendorfer, G., Pichler, H., Dwyer, J., & Rahman, M. (2018). X-ray observations at gaisberg tower. *Atmosphere*, *9*(1), 20. <https://doi.org/10.3390/atmos9010020>
- Hill, J. D. (2012). *The mechanisms of lightning leader propagation and ground attachment*. University of Florida.
- Howard, J., Uman, M. A., Biagi, C., Hill, D., Jerauld, J., Rakov, V. A., et al. (2010). Rf and x-ray source locations during the lightning attachment process. *Journal of Geophysical Research*, *115*(D6). <https://doi.org/10.1029/2009jd012055>
- Howard, J., Uman, M. A., Dwyer, J. R., Hill, D., Biagi, C., Saleh, Z., et al. (2008). Co-location of lightning leader x-ray and electric field change sources. *Geophysical Research Letters*, *35*(13). <https://doi.org/10.1029/2008gl034134>
- Hubbell, J. H., & Seltzer, S. M. (1995). *Tables of x-ray mass attenuation coefficients and mass energy-absorption coefficients 1 keV to 20 MeV for elements Z = 1 to 92 and 48 additional substances of dosimetric interest (Tech. Rep.)*. National Inst. of Standards and Technology-PL. <https://dx.doi.org/10.18434/T4D01F>
- Kochkin, P., van Deursen, A., Marisaldi, M., Ursi, A., de Boer, A., Bardet, M., et al. (2017). In-flight observation of gamma ray glows by ildas. *Journal of Geophysical Research: Atmosphere*, *122*(23), 12–801. <https://doi.org/10.1002/2017jd027405>
- Kochkin, P., van Deursen, A. P., & Ebert, U. (2014). Experimental study on hard x-rays emitted from meter-scale negative discharges in air. *Journal of Physics D: Applied Physics*, *48*(2), 025205. <https://doi.org/10.1088/0022-3727/48/2/025205>
- Lyu, F., Cummer, S. A., Krehbiel, P. R., Rison, W., Briggs, M. S., Cramer, E., et al. (2018). Very high frequency radio emissions associated with the production of terrestrial gamma-ray flashes. *Geophysical Research Letters*, *45*(4), 2097–2105. <https://doi.org/10.1002/2018gl077102>
- Mallick, S., Rakov, V., & Dwyer, J. R. (2012). A study of x-ray emissions from thunderstorms with emphasis on subsequent strokes in natural lightning. *Journal of Geophysical Research*, *117*(D16). <https://doi.org/10.1029/2012jd017555>
- Marisaldi, M., Fuschino, F., Tavani, M., Dietrich, S., Price, C., Galli, M., et al. (2014). Properties of terrestrial gamma ray flashes detected by agile mcal below 30 MeV. *Journal of Geophysical Research Space Physics*, *119*(2), 1337–1355. <https://doi.org/10.1002/2013ja019301>
- Montanyà, J., Fabró, F., March, V., van der Velde, O., Solà, G., Romero, D., & Argemí, O. (2015). X-rays and microwave rf power from high voltage laboratory sparks. *Journal of Atmospheric and Solar-Terrestrial Physics*, *136*, 94–97. <https://doi.org/10.1016/j.jastp.2015.06.009>
- Montanyà, J., Fabró, F., van der Velde, O., Romero, D., Solà, G., Hermoso, J. R., et al. (2014). Registration of x-rays at 2500 m altitude in association with lightning flashes and thunderstorms. *Journal of Geophysical Research-D: Atmospheres*, *119*(3), 1492–1503. <https://doi.org/10.1002/2013jd021011>
- Montanyà, J., Van der Velde, O. A., March, V., Romero, D., Solà, G., & Pineda, N. (2012). High-speed video of lightning and x-ray pulses during the 2009–2010 observation campaigns in northeastern Spain. *Atmospheric Research*, *117*, 91–98. <https://doi.org/10.1016/j.atmosres.2011.09.013>
- Moore, C. B., Eack, K. B., Aulich, G. D., & Rison, W. (2001). Energetic radiation associated with lightning stepped-leaders. *Geophysical Research Letters*, *28*(11), 2141–2144. <https://doi.org/10.1029/2001gl013140>
- Moss, G. D., Pasko, V. P., Liu, N., & Veronis, G. (2006). Monte carlo model for analysis of thermal runaway electrons in streamer tips in transient luminous events and streamer zones of lightning leaders. *Journal of Geophysical Research*, *111*(A2). <https://doi.org/10.1029/2005ja011350>
- Nemiroff, R. J., Bonnell, J. T., & Norris, J. P. (1997). Temporal and spectral characteristics of terrestrial gamma flashes. *Journal of Geophysical Research*, *102*(A5), 9659–9665. <https://doi.org/10.1029/96ja03107>
- Neubert, T., Østgaard, N., Reglero, V., Chanrion, O., Heumesser, M., Dimitriadou, K., et al. (2020). A terrestrial gamma-ray flash and ionospheric ultraviolet emissions powered by lightning. *Science*, *367*(6474), 183–186. <https://doi.org/10.1126/science.aax3872>
- Østgaard, N., Gjesteland, T., Hansen, R., Collier, A., & Carlson, B. (2012). The true fluence distribution of terrestrial gamma flashes at satellite altitude. *Journal of Geophysical Research*, *117*(A3). <https://doi.org/10.1029/2011ja017365>
- Østgaard, N., Gjesteland, T., Stadsnes, J., Connell, P., & Carlson, B. (2008). Production altitude and time delays of the terrestrial gamma flashes: Revisiting the burst and transient source experiment spectra. *Journal of Geophysical Research*, *113*(A2). <https://doi.org/10.1029/2007ja012618>
- Roberts, C., Marisaldi, M., Lindanger, A., Østgaard, N., Ursi, A., Sarria, D., et al. (2020). The 3rd agile terrestrial gamma-ray flashes catalog. Part II: Optimized selection criteria and characteristics of the new sample. *Journal of Geophysical Research: Atmosphere*, *125*(11), e2019JD031986. <https://doi.org/10.1029/2019JD031986>
- Saba, M., Ferro, M., Cuadros, E., Custódio, D., Nag, A., Schumann, C., et al. (2019). High-speed video observation of a dart leader producing x-rays. *Journal of Geophysical Research: Space Physics*, *124*(12), 9755–10815.
- Saleh, Z., Dwyer, J. R., Howard, J., Uman, M., Bakhtiari, M., Concha, D., et al. (2009). Properties of the x-ray emission from rocket-triggered lightning as measured by the thunderstorm energetic radiation array (tera). *Journal of Geophysical Research*, *114*(D17). <https://doi.org/10.1029/2008jd011618>

- Schaal, M., Dwyer, J. R., Rassoul, H. K., Hill, J. D., Jordan, D. M., & Uman, M. A. (2013). The angular distribution of energetic electron and x-ray emissions from triggered lightning leaders. *Journal of Geophysical Research: Atmosphere*, *118*(20), 11–712. <https://doi.org/10.1002/2013jd019619>
- Shao, X.-M., Hamlin, T., & Smith, D. M. (2010). A closer examination of terrestrial gamma-ray flash-related lightning processes. *Journal of Geophysical Research*, *115*(A6). <https://doi.org/10.1029/2009ja014835>
- Skeie, C., Østgaard, N., Lehtinen, N., Sarria, D., Kochkin, P., de Boer, A., et al. (2020). Constraints on recoil leader properties estimated from x-ray emissions in aircraft-triggered discharges. *Journal of Geophysical Research: Atmosphere*, *125*(14), e2019JD032151. <https://doi.org/10.1029/2019jd032151>
- Skeltved, A. B., Østgaard, N., Carlson, B., Gjesteland, T., & Celestin, S. (2014). Modeling the relativistic runaway electron avalanche and the feedback mechanism with geant4. *Journal of Geophysical Research Space Physics*, *119*(11), 9174–9191. <https://doi.org/10.1002/2014ja020504>
- Smith, D., Bowers, G., Kamogawa, M., Wang, D., Ushio, T., Ortberg, J., et al. (2018). Characterizing upward lightning with and without a terrestrial gamma ray flash. *Journal of Geophysical Research: Atmosphere*, *123*(20), 11–321. <https://doi.org/10.1029/2018jd029105>
- Smith, D., Dwyer, J., Hazelton, B., Grefenstette, B., Martinez-McKinney, G., Zhang, Z., et al. (2011). A terrestrial gamma ray flash observed from an aircraft. *Journal of Geophysical Research*, *116*(D20). <https://doi.org/10.1029/2011jd016252>
- Stock, M. G., Akita, M., Krehbiel, P. R., Rison, W., Edens, H. E., Kawasaki, Z., & Stanley, M. A. (2014). Continuous broadband digital interferometry of lightning using a generalized cross-correlation algorithm. *Journal of Geophysical Research - D: Atmospheres*, *119*(6), 3134–3165. <https://doi.org/10.1002/2013jd020217>
- Tran, M., & Rakov, V. (2017). A study of the ground-attachment process in natural lightning with emphasis on its breakthrough phase. *Scientific Reports*, *7*(1), 1–13. <https://doi.org/10.1038/s41598-017-14842-7>
- Tierney, H. E., Roussel-Dupré, R. A., Symbalysty, E. M., & Beasley, W. H. (2005). Radio frequency emissions from a runaway electron avalanche model compared with intense, transient signals from thunderstorms. *Journal of Geophysical Research*, *110*(D12). <https://doi.org/10.1029/2004jd005381>
- Tran, M. D., Kereszy, I., Rakov, V. A., & Dwyer, J. R. (2019). On the Role of Reduced Air Density Along the Lightning Leader Path to Ground in Increasing X-Ray Production Relative to Normal Atmospheric Conditions. *Geophysical Research Letters*, *46*(15), 9252–9260. <https://doi.org/10.1029/2019gl083753>
- Tran, M. D., Rakov, V. A., Mallick, S., Dwyer, J. R., Nag, A., Heckman, S. (2015). A terrestrial gamma-ray flash recorded at the lightning observatory in Gainesville, Florida. *Journal of Atmospheric and Solar-Terrestrial Physics*, *136*, 86–93. <https://doi.org/10.1016/j.jastp.2015.10.010>
- Von Kienlin, A., Meegan, C. A., Paciesas, W. S., Bhat, P. N., Bissaldi, E., Briggs, M. S., et al. (2014). The second fermi gbm gamma-ray burst catalog: The first four years. *The Astrophysical Journal*, *211*(1), 13. <https://doi.org/10.1088/0067-0049/211/1/13>
- Wada, Y., Enoto, T., Nakamura, Y., Furuta, Y., Yuasa, T., Nakazawa, K., et al. (2019). Gamma-ray glow preceding downward terrestrial gamma-ray flash. *Communications on Physics*, *2*(1), 1–9. <https://doi.org/10.1038/s42005-019-0168-y>
- Williams, E., Boldi, R., Bor, J., Satori, G., Price, C., Greenberg, E., et al. (2006). Lightning flashes conducive to the production and escape of gamma radiation to space. *Journal of Geophysical Research*, *111*(D16). <https://doi.org/10.1029/2005jd006447>